TABLE I – IC_{50} VALUES OF SN-38, NK012, CPT-11, ACNU, CDDP AND VP-16 IN VARIOUS HUMAN GLIOBLASTOMA CELL LINES

Cell line	IC_{50}(μmol/l)					
	SN38	NK012	CPT-11	ACNU	CDDP	Etoposide
LN18	0.052 ± 0.0034	0.069 ± 0.0242	13.0 ± 0.88	729 ± 30	3.57 ± 0.08	3.84 ± 0.14
LN229	0.28 ± 0.1094	0.36 ± 0.0489	12.2 ± 1.23	144 ± 23	21.4 ± 0.62	0.945 ± 0.025
U87MG	0.18 ± 0.0216	0.093 ± 0.0038	18.1 ± 3.06	865 ± 86	9.06 ± 0.57	20.8 ± 5.23
U118MG	0.0089 ± 0.0003	0.022 ± 0.0017	4.85 ± 0.14	282 ± 22	3.35 ± 0.35	4.05 ± 0.18
U251MG	0.0076 ± 0.0001	0.0087 ± 0.0002	3.86 ± 0.04	51.6 ± 3.7	4.55 ± 0.03	2.42 ± 0.13

Each cell line was treated in triplicate for 72 hr.
WST–8 assay was used for obtaining IC_{50} value.

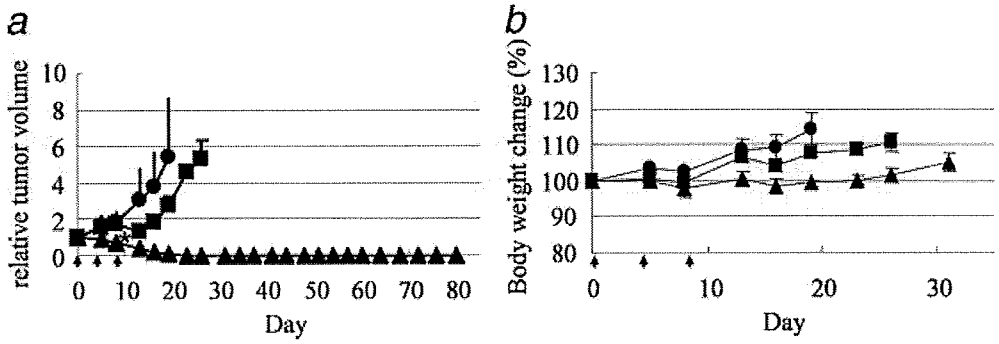

FIGURE 1 – Effects of NK012 and CPT-11 on U87MG/Luc tumor xenograft. (*a*) Tumor volume in mice treated with CPT-11 or NK012. U87MG/Luc tumor was subcutaneously inoculated into the flank of mice, as described in the Materials and methods section. NaCl (0.9%) solution (●), CPT-11 at 66.7 mg/kg (■) and NK012 at 30 mg/kg (▲) were intravenously administered on days 0, 4 and 8 (arrows). Points, mean; bars, SD. *$p < 0.05$. (*b*) Treatment-related body weight loss occurred in mice treated with CPT-11 and NK012. Points, mean; bars, SD.

samples were diluted with 20 μl of methanol (50%, v/v) and 20 μl of NaOH (0.3 mol/l for plasma and 0.7 mol/l for tissue). The samples were incubated for 15 min at 25°C. After incubation, 20 μl of HCl (0.3 mol/l for plasma and 0.7 mol/l for tissue) and 60 μl of CPT solution (10 ng/ml for SN-38 and 15 ng/ml for CPT-11) were added to the samples, and then the hydrolysate was filtered through a MultiScreen Solvinert. Fifty microliters of the filtrate was applied to the same HPLC system as described earlier.

In vivo *growth inhibition assay*

Experiment 1. Six-week-old mice were subcutaneously inoculated with 1×10^7 U87MG/Luc cells in the flank region. When tumor volume reached ~605 mm^3, mice were randomly divided into test groups consisting of 3 mice per group (day 0). Drug was intravenously administered on days 0, 4 and 8 into the tail vein. NK012 was administered at its MTD of 30 mg/kg/day. The reference drug CPT-11 was given at its MTD of 66.7 mg/kg/day in the optimal schedule reported.[17,21] The length (*i*) and width (*ii*) of tumor masses were measured twice a week, and tumor volume (TV) was calculated as follows: $TV = (a \times b^2)/2$. Relative tumor volumes (RTVs) at day n were calculated according to the following formula: $RTV = TV_n / TV_0$, where TV_n is the tumor volume at day n, and TV_0 is the tumor volume at day 0.

Experiment 2. To assess the antitumor effect of NK012 and CPT-11, *in vivo* bioluminescence imaging studies were performed using the Photon Imager animal imaging system (Biospace, Paris, France). For imaging, mice with intracranial U87MG/Luc tumor were simultaneously anesthetized with isoflurane and d-luciferine potassium salt (Synchem, Germany), and normal 0.9% NaCl solution was intraperitoneally administrated at a dose of 125 mg/kg body weight, and images were obtained 5 min after the injection. For bioluminescence image analysis, regions of interest encompassing the intracranial area of a signal were defined using Photo Vision software (Biospace, Paris, France), and total numbers of photons per minute (cpm) were recorded. The pseudo-color luminescent image from violet (least intense) to red (most intense) represented the spatial distribution of detected photon counts emerging from active luciferase within the animal. Twenty days after U87MG inoculation, treatment was started (day 0). Normal 0.9% NaCl solution ($n = 4$), NK012 (30 mg/kg, $n = 4$), or CPT-11 (66.7 mg/kg, $n = 4$) was intravenously administered to mice on days 0, 4 and 8. *In vivo* bioluminescence imaging studies were performed on days 0, 14, 21 and 28 from the day of treatment initiation. To determine the effect of treatment on the time to change of intensity, Student's *t* test was carried out using the StatView 5.0 software package. $p < 0.05$ was regarded as significant.

Experiment 3. Mice with intracranial U87MG/Luc tumor was randomly divided into 3 groups consisting of 6 mice per group. NK012 (30 mg/kg/day) and CPT-11 (66.7 mg/kg/day) were intravenously given on days 0 (20 days after tumor inoculation), 4 and 8. After treatment, mice were maintained until each animal showed signs of morbidity (*i.e.*, 10% weight loss and neurological deficit), at which point they were sacrificed. Kaplan-Meier analysis was performed to determine the effect of drugs on time to morbidity, and statistical differences were ranked according to the Mantel-Cox log-rank test using StatView 5.0.

Statistical analysis

Data were expressed as mean ± SD. Significance of differences was calculated using the unpaired *t* test with repeated measures of StatView 5.0. $p < 0.05$ was regarded as significant.

Results

Cellular sensitivity of glioblastoma cells to SN-38, NK012 and CPT-11

The IC_{50} values of NK012 for the cell lines ranged from 0.0087 μmol/l (U251MG cells) to 0.36 μmol/l (LN229 cells). The growth inhibitory effects of NK012 were 34- to 444-fold more potent than those of CPT-11, 400- to 12818-fold more potent than those of ACNU, 52-to 523-fold more potent than those of CDDP, and 3- to 278-fold

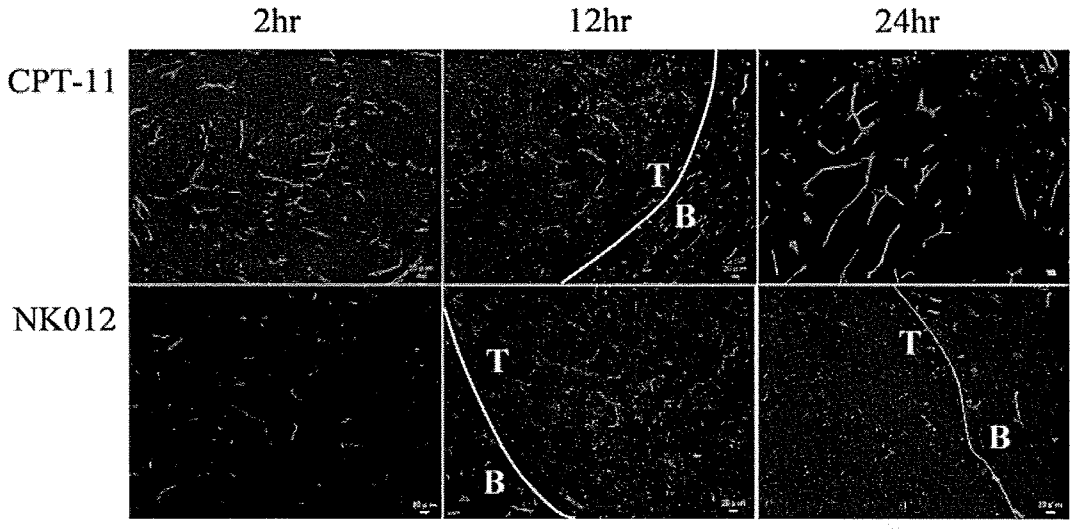

FIGURE 2 – Distribution of NK012 or CPT-11 in U87MG/Luc glioma xenografts. Mice bearing U87MG/Luc tumor were injected with NK012 (30 mg/kg/day) or CPT-11 (66.7 mg/kg/day). Tumor tissues were excised 2, 12 and 24 hr after the intravenous injection of NK012 or CPT-11. Each mouse was administered fluorescein-labeled *Lycopersicon esculentum* lectin 5 min before sacrifice to detect tumor blood vessels. Frozen sections were examined under a fluorescence microscope at an excitation wavelength of 377 nm and an emission wavelength of 477 nm. The same fluorescence conditions can be applied for visualizing NK012 and CPT-11 fluorescence. Free SN-38 could not be detected under these fluorescence conditions. The white lines indicate the border between the tumor and the brain tissue. T, U87MG/Luc tumor; B, normal brain tissue. (Scale bars: 20 μm).

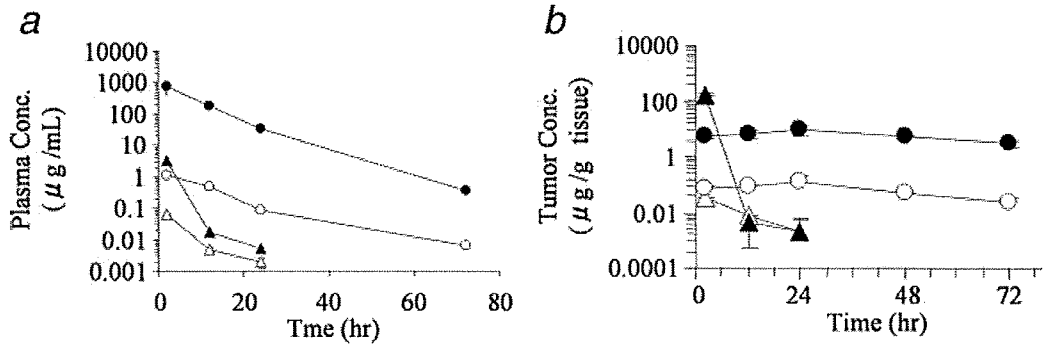

FIGURE 3 – Plasma, brain tissue and orthotopic tumor concentrations of respective analytes after intravenous administration of NK012 (30 mg/kg/day) and CPT-11 (66.7 mg/kg/day) to U87MG/Luc-bearing nude mice. (*a*) plasma; (*b*) tumor. ●, polymer-bound SN-38; ○, free SN-38 (polymer-unbound SN-38); ▲, CPT-11; Δ, free SN-38 converted from CPT-11.

more potent than those of etoposide. On the other hand, the IC_{50} values of NK012 were almost similar to those of SN-38 (Table. I).

Antitumor activity of NK012 and CPT-11 on subcutaneous U87MG/Luc xenografts

Potent antitumor activity was observed in mice treated with NK012 at 30 mg/kg *in vivo* (Fig. 1*a*). In mice treated with NK012, tumor volume started to decrease on day 5, and the tumor completely disappeared by day 23, with no relapse observed until 80 days after treatment. Although CPT-11 at 66.7 mg/kg/day exerted antitumor activity compared with the control group, tumor volume continued to increase consistently. Comparison of the relative tumor volume at day 8 revealed significant differences between the NK012-treated and CPT-11-treated groups ($p = 0.0095$). Although treatment-related body weight loss was observed in mice treated with each drug, body weight recovery was observed by day 19 (Fig. 1*b*). These results clearly show the significant *in vivo* activity of NK012 against the U87MG/Luc tumor xeonograft.

Studies on distribution of NK012 and CPT-11 in orthotopic U87MG/Luc tumor tissues

Both NK012 and CPT-11 formulations accumulated in the tumor tissue but not in the normal brain tissue (Fig. 2). However, the drug distribution pattern was clearly different between NK012 and CPT-11. In sections of the U87MG/Luc tumor treated with CPT-11, maximum drug accumulation was observed within 2 hr of CPT-11 injection. Twelve hours after the injection, fluorescence originating from CPT-11 had almost disappeared. Subsequently, no accumulation of CPT-11 was observed within the tumor tissues. However, in sections of the U87MG/Luc tumor treated with NK012, fluorescence from NK012 started appearing around tumor blood vessels 2 hr after intravenous injection and lasted until 24

TABLE II – TUMOR AND PLASMA CONCENTRATION OF SN38 AFTER AN I.V. ADMINISTRATION OF NK012 (30 MG/KG) AND CPT-11 (66.7MG/KG) TO NUDE MICE BEARING U87MG/LUC BRAIN TUMOR

Formulation tested	Analyte		Time after administration (hr)			
			2	12	24	72
NK012	Free SN-38	Plasma (ng/ml)	1113	511	90.0	6.88
		Tumor (ng/g)	67.7	84.1	137	24.6
CPT-11	Free SN-38 5	Plasma (ng/ml)	62.0	4.74	1.97	ND
		Tumor (ng/g)	31.8	7.41	2.14	ND

Data were expressed as means of three mice.
Free SN-38; SN-38 released from NK012 or converted from CPT-11.
ND, not detectable.

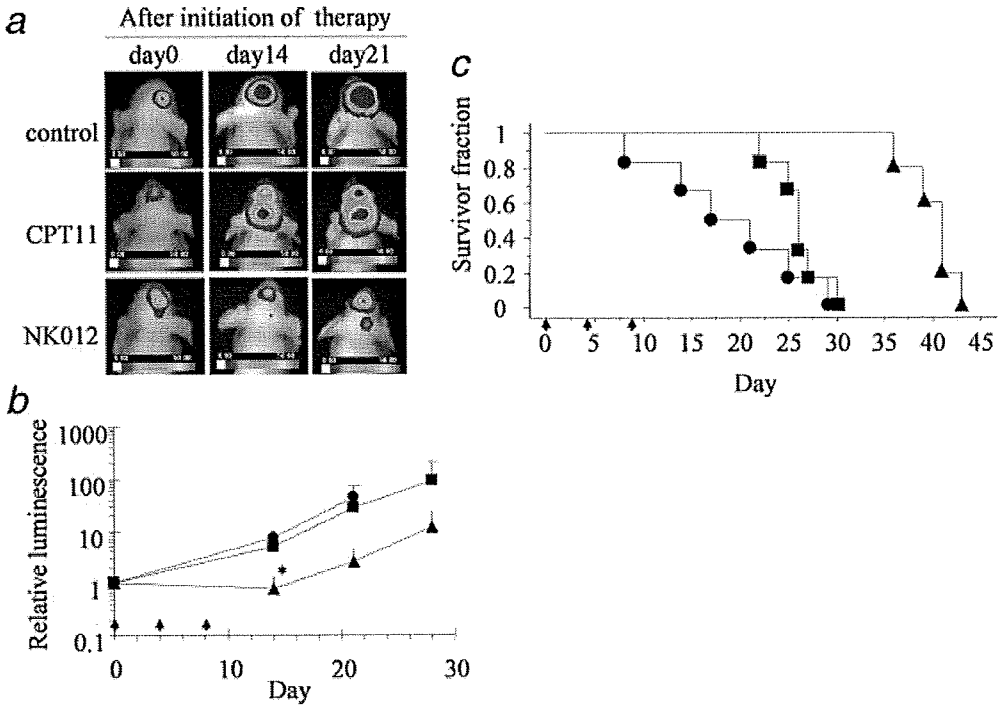

FIGURE 4 – Antitumor effect of NK012 or CPT-11 on orthotopic xenograft and survival. Mice receiving intracranial injections of U87MG/Luc were assigned into groups 20 days after tumor inoculation. Mice were intravenously administered with 0.9% NaCl solution (●), NK012 (30 mg/kg/day, ▲) or CPT-11 (66.7 mg/kg/day, ■) on days 0 (20 days after tumor inoculation), 4 and 8 (arrows). (*a*) Representative luminescence intensity images obtained in individual control and treatment-group mice on the days indicated. (*b*) Antitumor effect of NK012 or CPT-11 on days 14, 21 and 28. Each group consisted of 4 mice. Points, mean; bars, SD. $*p < 0.05$. (*c*) Treatment effects of NK012 on survival. Survival was assessed by Kaplan-Meier analysis. Each group consisted of 6 mice. Experiments were repeated twice with similar results.

hr. After 12 hr, the fluorescent area began to increase and the maximum fluorescence area was observed 24 hr after the injection.

Pharmacokinetics analysis of NK012 and CPT-11 in mice bearing orthotopic U87MG/Luc xenografts

Microscopic observations were confirmed quantitatively by measuring the amount of SN-38 extracted from each solid tumor by reversed-phase HPLC. After CPT-11 injection, the concentrations of CPT-11 and free SN-38 in plasma decreased rapidly with time in a log-linear fashion. On the other hand, the plasma concentration of NK012 (polymer-bound SN-38) showed slower clearance than that of CPT-11. Free SN-38 released from NK012 also showed slow clearance than that of SN-38 converted from CPT-11 (Fig. 3*a*). Meanwhile, there was a significant difference in drug accumulation in the tumor between CPT-11 and NK012, that is, the accumulation of NK012 in the U87MG/Luc tumor was significantly higher than that of CPT-11 (Fig. 3*b*) and that the concentration of free SN-38 originating from NK012 was maintained at 24.6 ng/g even 72 hr after injection (Table II). On the other hand, only slight conversion from CPT-11 to SN-38 was observed from 2 to 24 hr in the U87MG/Luc tumor, and no SN-38 was detected thereafter (Fig. 3*b*). This result suggests that the BTB of the tumor was partially destroyed in the tumor vasculature and both drugs extravasated from the tumor blood vessels. In addition, these results indicate that NK012 can remain in the tumor tissue for a longer period and continue to release free SN-38.

Antitumor activity of NK012 and CPT-11 against orthotopic U87MG/Luc glioma xenografts

Antitumor activity was observed in mice treated with NK012 at 30 mg/kg/day and CPT-11 at 66.7 mg/kg/day *in vivo* (Fig. 4*a*). ANOVA analysis revealed a significant difference between the control group and the NK012-treated group ($p = 0.02$). However there was no significant difference between the control group and

the CPT-11-treated group ($p = 0.23$) and between NK012 and CPT-11 ($p = 0.21$) (Fig. 4*b*). Comparison of the relative tumor volume at day 14 revealed significant differences between NK012 (30 mg/kg/day) and CPT-11 (66.7 mg/kg/day) ($p = 0.049$). Kaplan-Meier analysis showed that a significant improvement in survival rate was observed in the NK012 treatment group compared with the control ($p = 0.001$) and CPT-11 treatment groups ($p = 0.0014$) (Fig. 4*c*).

Discussion

The diameter of a micelle carrier is approximately in the range of 10–100 nm, which is smaller than that of a liposome. Although this size is small, it is still sufficiently large to prevent renal secretion of the carrier. The micelle systems can evade nonspecific capture by the reticuloendothelial system in various organs because the outer shell of the micelle is covered with polyethyleneglycol. Therefore, drug-incorporating micelles can be expected to have a long plasma half-life, which permits a large amount of the micelles to reach tumor tissues, extravasate from tumor capillaries, and then be retained in tumor tissues for a long time by utilizing the enhanced permeability and retention (EPR) effect.[22]

Several factors are reportedly involved in vascular permeability in the body. Among them, bradykinin is the most potent vascular permeability factor. We succeeded in purifying 2 types of kinin from the ascitic fluid of a patient with gastric cancer.[23] We also clarified that this kinin generation system was triggered by the activated Hageman factor, an intrinsic coagulation factor XII.[24] Meanwhile, Dvorak et al. discovered that the vascular permeability factor (VPF) is involved in tumor vascular permeability.[25] Later, it was found that VPF was identical to VEGF.[26] Recently, an extrinsic coagulation factor, namely, a tissue factor, has been shown to activate VEGF production.[27,28] Thus, both intrinsic and extrinsic coagulation factors may be involved in tumor vascular permeability. Furthermore, there have been several reports to date indicating the increasing expression of a tissue factor in human glioma.[29,30] Also, it is well known that glioma is a typical hypervascular tumor with an irregular vascular architecture and a high expression level of VEGF.[31] Therefore, it may be speculated that nanoparticles extravasate from tumor capillaries and accumulate more preferentially in brain glioma.

NK012, an SN-38-incorporating polymeric micelle, is a novel type of micellar formulation with long-time accumulation in tumors, and shows prolonged sustained release of SN-38 within the tumor.[17,20] We have thus far reported that NK012 shows significantly higher antitumor activity against various human tumor xenografts including small cell lung cancer,[17] colorectal cancer,[19] renal cancer,[18] and pancreatic cancer[20] compared with CPT-11. In addition, we have recently seen an increasing number of reports of clinical trials indicating the effectiveness of CPT-11 against brain glioma in combination with anti-VEGF antibody[11,12,32,33]

Under these circumstances, it may be reasonable to conduct an investigation into the advantages of administering NK012 over CPT-11 for treatment against human glioma tumor xenografts. In the present study, we showed that NK012 exerted a significant antitumor activity in U87MG/Luc subcutaneous xenografts (Fig. 1). In the tumor intravenously administered with NK012 (30 mg/kg), NK012 accumulated within and around tumor blood vessels in the orthotopic xenografts 2 hr after the injection. Thereafter, NK012 started to spread from the blood vessel within the tumor tissue of the xenografts. Fluorescence originating from NK012 then increased up to the maximum in the entire tumor by 24 hr after NK012 injection. On the other hand, fluorescence originating from CPT-11 increased up to the maximum 2 hr after its injection, indicating that the maximum distribution of CPT-11 was achieved within 2 hr of injection. Twelve hours after intravenous injection, fluorescence from CPT-11 had almost disappeared, and subsequently, no accumulation of CPT-11 was observed within the tumor tissues. The therapeutic effect of NK012 was superior to that of CPT-11 in terms of antitumor effect and survival. Because the antitumor activity of SN-38 is time-dependent, the superiority of NK012 over CPT-11 may be due to the enhanced accumulation of NK012 and the prolonged sustained release of SN-38 from NK012 within the tumor tissues. Nevertheless, free SN-38 was not detected in the normal brain tissues at any measurement time after intravenous injection of NK012 or CPT-11 (data not shown). It is thus speculated that both NK012 and CPT-11 are unable to cross the BBB in the normal brain, but can pass through tumor vessels effectively. In clinical brain glioma, however, when the tumor recurs, it would most likely recur in adjacent regions of the brain with an intact blood brain barrier. Namely, at the border between the brain tumor and normal brain tissue, malignant glioma cells and normal brain tissues intermix in the gradient and angiogenesis occurs at sites where there are large accumulation of tumor cells under local hypoxia.[34] In addition, there is no clear evidence if tumor vessels of orthotopic brain tumor xenografts are identical to those of real human brain tumors in terms of their structure and function. Therefore, it may be better to consider to conduct an investigation of the advantages of administering some anti-angiogenic inhibitors in combination with NK012 against highly invasive tumor models established by several methods such as direct implantation of patient surgical specimens into the brains of nude mice,[35] transplantation of patient surgical material s.c. in nude mice followed by dissociation and orthotopic reinjection of these xenotransplants,[36] engraftment of glioblastoma-derived spheroids after short- term culture into rat brain,[37] and engraftment of glioblastomastem cell-enriched cultures into mouse brain.[38,39]

The dose-limiting toxicities of CPT-11 appeared to be neutropenia and diarrhea. However, in our previous data, there was no significant difference in the level of SN-38 in the small intestine between NK012-treated and CPT-11-treated mice.[17] It was also reported that NK012 showed significant antitumor effect with diminishing incidence of diarrhea compared with CPT-11.[40] In 2 individual phase 1 trials in Japan and the US, no serious diarrhea has been reported.[41,42] In addition, one confirmed partial response (PR) was obtained in a patient with metastatic esophageal cancer in a Japanese trial,[41] and 3 PRs in a patient with breast cancer and 1 PR in a patient with small cell lung cancer in a US phase 1 trial.[42]

In conclusion, we demonstrated not only the enhanced accumulation, distribution, and retention of NK012 within glioma xenografts but also the superiority of the antitumor activity of NK012 compared with CPT-11. Taking the present data together with very recent clinical data from phase 1 trials, a phase 2 trial in patients with recurrent glioma may be warranted.

Acknowledgements

The authors thank Ms. N. Mie, Ms. H. Miyatake and Ms. M. Ohtsu for their technical assistance and Ms. K. Shiina for her secretarial assistance.

References

1. DeAngelis LM. Brain tumors. N Engl J Med 2001;344:114–23.
2. Kleihues P, Louis DN, Scheithauer BW, Rorke LB, Reifenberger G, Burger PC, Cavenee WK. The WHO classification of tumors of the nervous system. J Neuropathol Exp Neurol 2002;61:215–25 discussion 26–9.
3. Stupp R, Mason WP, van den Bent MJ, Weller M, Fisher B, Taphoorn MJ, Belanger K, Brandes AA, Marosi C, Bogdahn U, Curschmann J, Janzer RC, et al. Radiotherapy plus concomitant and adjuvant temozolomide for glioblastoma. N Engl J Med 2005;352:987–96.
4. Wong ET, Hess KR, Gleason MJ, Jaeckle KA, Kyritsis AP, Prados MD, Levin VA, Yung WK. Outcomes and prognostic factors in recurrent glioma patients enrolled onto phase II clinical trials. J Clin Oncol 1999;17:2572–8.

5. Li LH, Fraser TJ, Olin EJ, Bhuyan BK. Action of camptothecin on mammalian cells in culture. Cancer Res 1972;32:2643–50.
6. Gallo RC, Whang-Peng J, Adamson RH. Studies on the antitumor activity, mechanism of action, and cell cycle effects of camptothecin. J Natl Cancer Inst 1971;46:789–95.
7. Friedman HS, Petros WP, Friedman AH, Schaaf LJ, Kerby T, Lawyer J, Parry M, Houghton PJ, Lovell S, Rasheed K, Cloughsey T, Stewart ES, et al. Irinotecan therapy in adults with recurrent or progressive malignant glioma. J Clin Oncol 1999;17:1516–25.
8. Cloughesy TF, Filka E, Kuhn J, Nelson G, Kabbinavar F, Friedman H, Miller LL, Elfring GL. Two studies evaluating irinotecan treatment for recurrent malignant glioma using an every-3-week regimen. Cancer 2003;97:2381–6.
9. Chamberlain MC. Salvage chemotherapy with CPT-11 for recurrent glioblastoma multiforme. J Neurooncol 2002;56:183–8.
10. Prados MD, Lamborn K, Yung WK, Jaeckle K, Robins HI, Mehta M, Fine HA, Wen PY, Cloughesy T, Chang S, Nicholas MK, Schiff D, et al. A phase 2 trial of irinotecan (CPT-11) in patients with recurrent malignant glioma: a North American brain tumor consortium study. Neuro Oncol 2006;8:189–93.
11. Vredenburgh JJ, Desjardins A, Herndon JE, II, Dowell JM, Reardon DA, Quinn JA, Rich JN, Sathornsumetee S, Gururangan S, Wagner M, Bigner DD, Friedman AH, et al. Phase II trial of bevacizumab and irinotecan in recurrent malignant glioma. Clin Cancer Res 2007;13: 1253–9.
12. Vredenburgh JJ, Desjardins A, Herndon JE, II, Marcello J, Reardon DA, Quinn JA, Rich JN, Sathornsumetee S, Gururangan S, Sampson J, Wagner M, Bailey L, et al. Bevacizumab plus irinotecan in recurrent glioblastoma multiforme. J Clin Oncol 2007;25:4722–9.
13. Gradishar WJ. Albumin-bound nanoparticle paclitaxel. Clin Adv Hematol Oncol 2005;3:348–9.
14. Muggia FM. Liposomal encapsulated anthracyclines: new therapeutic horizons. Curr Oncol Rep 2001;3:156–62.
15. Slatter JG, Schaaf LJ, Sams JP, Feenstra KL, Johnson MG, Bombardt PA, Cathcart KS, Verburg MT, Pearson LK, Compton LD, Miller LL, Baker DS, et al. Pharmacokinetics, metabolism, and excretion of irinotecan (CPT-11) following I.V. infusion of [(14)C]CPT-11 in cancer patients. Drug Metab Dispos 2000;28:423–33.
16. Rothenberg ML, Kuhn JG, Burris HA, III, Nelson J, Eckardt JR, Tristan-Morales M, Hilsenbeck SG, Weiss GR, Smith LS, Rodriguez GI, et al. Phase I and pharmacokinetic trial of weekly CPT-11. J Clin Oncol 1993;11:2194–204.
17. Koizumi F, Kitagawa M, Negishi T, Onda T, Matsumoto S, Hamaguchi T, Matsumura Y. Novel SN-38-incorporating polymeric micelles, NK012, eradicate vascular endothelial growth factor-secreting bulky tumors. Cancer Res 2006;66:10048–56.
18. Sumitomo M, Koizumi F, Asano T, Horiguchi A, Ito K, Kakizoe T, Hayakawa M, Matsumura Y. Novel SN-38-incorporated polymeric micelle, NK012, strongly suppresses renal cancer progression. Cancer Res 2008;68:1631–5.
19. Nakajima TE, Yasunaga M, Kano Y, Koizumi F, Kato K, Hamaguchi T, Yamada Y, Shirao K, Shimada Y, Matsumura Y. Synergistic antitumor activity of the novel SN-38-incorporating polymeric micelles, NK012, combined with 5-fluorouracil in a mouse model of colorectal cancer, as compared with that of irinotecan plus 5-fluorouracil. Int J Cancer 2008;122:2148–53.
20. Saito Y, Yasunaga M, Kuroda J, Koga Y, Matsumura Y. Enhanced distribution of NK012, a polymeric micelle-encapsulated SN-38, and sustained release of SN-38 within tumors can beat a hypovascular tumor. Cancer Sci 2008;99:1258–64.
21. Kawato Y, Furuta T, Aonuma M, Yasuoka M, Yokokura T, Matsumoto K. Antitumor activity of a camptothecin derivative, CPT-11, against human tumor xenografts in nude mice. Cancer Chemother Pharmacol 1991;28:192–8.
22. Matsumura Y, Maeda H. A new concept for macromolecular therapeutics in cancer chemotherapy: mechanism of tumoritropic accumulation of proteins and the antitumor agent smancs. Cancer Res 1986; 46:6387–92.
23. Maeda H, Matsumura Y, Kato H. Purification and identification of [hydroxyprolyl3]bradykinin in ascitic fluid from a patient with gastric cancer. J Biol Chem 1988;263:16051–4.
24. Matsumura Y, Maruo K, Kimura M, Yamamoto T, Konno T, Maeda H. Kinin-generating cascade in advanced cancer patients and in vitro study. Jpn J Cancer Res 1991;82:732–41.
25. Dvorak HF, Nagy JA, Dvorak JT, Dvorak AM. Identification and characterization of the blood vessels of solid tumors that are leaky to circulating macromolecules. Am J Pathol 1988;133:95–109.
26. Leung DW, Cachianes G, Kuang WJ, Goeddel DV, Ferrara N. Vascular endothelial growth factor is a secreted angiogenic mitogen. Science 1989;246:1306–9.
27. Abe K, Shoji M, Chen J, Bierhaus A, Danave I, Micko C, Casper K, Dillehay DL, Nawroth PP, Rickles FR. Regulation of vascular endothelial growth factor production and angiogenesis by the cytoplasmic tail of tissue factor. Proc Natl Acad Sci USA 1999;96:8663–8.
28. Belting M, Dorrell MI, Sandgren S, Aguilar E, Ahamed J, Dorfleutner A, Carmeliet P, Mueller BM, Friedlander M, Ruf W. Regulation of angiogenesis by tissue factor cytoplasmic domain signaling. Nat Med 2004;10:502–9.
29. Rong Y, Post DE, Pieper RO, Durden DL, Van Meir EG, Brat DJ. PTEN and hypoxia regulate tissue factor expression and plasma coagulation by glioblastoma. Cancer Res 2005;65:1406–13.
30. Hamada K, Kuratsu J, Saitoh Y, Takeshima H, Nishi T, Ushio Y. Expression of tissue factor correlates with grade of malignancy in human glioma. Cancer 1996;77:1877–83.
31. Takano S, Yoshii Y, Kondo S, Suzuki H, Maruno T, Shirai S, Nose T. Concentration of vascular endothelial growth factor in the serum and tumor tissue of brain tumor patients. Cancer Res 1996;56:2185–90.
32. Chowdhary S, Wong ET. Bevacizumab combined with irinotecan for recurrent glioblastoma multiforme–improvement over available therapy? Nat Clin Pract Neurol 2008;4:242–3.
33. Chamberlain MC Bevacizumab plus irinotecan in recurrent glioblastoma. J Clin Oncol 2008;26:1012–3.
34. Plate KH, Breier G, Weich HA, Risau W. Vascular endothelial growth factor is a potential tumour angiogenesis factor in human gliomas in vivo. Nature 1992;359:845–8.
35. Horten BC, Basler GA, Shapiro WR. Xenograft of human malignant glial tumors into brains of nude mice. A histopatholgical study. J Neuropathol Exp Neurol 1981;40:493–511.
36. Giannini C, Sarkaria JN, Saito A, Uhm JH, Galanis E, Carlson BL, Schroeder MA, James CD. Patient tumor EGFR and PDGFRA gene amplifications retained in an invasive intracranial xenograft model of glioblastoma multiforme. Neuro Oncol 2005;7:164–76.
37. Engebraaten O, Hjortland GO, Hirschberg H, Fodstad O. Growth of precultured human glioma specimens in nude rat brain. J Neurosurg 1999;90:125–32.
38. Galli R, Binda E, Orfanelli U, Cipelletti B, Gritti A, De Vitis S, Fiocco R, Foroni C, Dimeco F, Vescovi A. Isolation and characterization of tumorigenic, stem-like neural precursors from human glioblastoma. Cancer Res 2004;64:7011–21.
39. Gunther HS, Schmidt NO, Phillips HS, Kemming D, Kharbanda S, Soriano R, Modrusan Z, Meissner H, Westphal M, Lamszus K. Glioblastoma-derived stem cell-enriched cultures form distinct subgroups according to molecular and phenotypic criteria. Oncogene 2008;27:2897–909.
40. Onda T, Nakamura I, Seno C, Matsumoto S, Kitagawa M, Okamoto K, Nishikawa K, Suzuki M. Superior antitumor activity of NK012, 7-etyhl-10-hydroxycamptothecin-incorporating micellar nanoparticle, to irinotecan [abstruct 3062]. Proc Am Assoc Cancer Res 2006;47:720s.
41. Kato K, Hamaguchi T, Shirao K, Shimada Y, Doi T, Ohtsu A, Matsumura Y, Yamada Y. Interim analysis of phase I study of NK012, polymer micelle SN-38, in patients with advanced cancer. Proc Am Soc Clin Oncol GI 2008 (Abstract no 485).
42. Burris HA, III, Infante JR, Spigel DR, Greco FA, Thompson DS, Matsumoto S, Kawamura S, Jones SF. A phase I dose-escalation study of NK012. Proc Am Soc Clin Oncol 2008 (Abstract no 2538).

Clinically relevant radioresistant cells efficiently repair DNA double-strand breaks induced by X-rays

Yoshikazu Kuwahara,[1] Li Li,[2] Taisuke Baba,[1] Hironobu Nakagawa,[1] Tsutomu Shimura,[1] Yoichiro Yamamoto,[1] Yasuhito Ohkubo[3] and Manabu Fukumoto[1,4]

[1]Department of Pathology, Institute of Development, Aging and Cancer, Tohoku University, Sendai 980-8575; [2]Guangdong Key Laboratory for Research and Development of National Drugs, Guangdong Medical College, Zhanjiang 524023, China; [3]Department of Radiopharmacology, Tohoku Pharmaceutical University, Sendai 981-8558, Japan

(Received July 3, 2008/Revised September 19, 2008; November 9, 2008/Accepted December 3, 2008/Online publication February 2, 2009)

Radiotherapy is one of the major therapeutic modalities for eradicating malignant tumors. However, the existence of radioresistant cells remains one of the most critical obstacles in radiotherapy and radiochemotherapy. Standard radiotherapy for tumor treatment consists of approximately 2 Gy once a day, 5 days a week, over a period of 5–8 weeks. To understand the characteristics of radioresistant cells and to develop more effective radiotherapy, we established a novel radioresistant cell line, HepG2-8960-R with clinical relevance from parental HepG2 cells by long-term fractionated exposure to 2 Gy of X-rays. HepG2-8960-R cells continued to proliferate with daily exposure to 2 Gy X-rays for more than 30 days, while all parental HepG2 cells ceased. After exposure to fractionated 2 Gy X-rays, induction frequencies of micronuclei and remaining foci of γ-H2AX in HepG2-8960-R were less than those in HepG2. Flow cytometric analysis revealed that the proportion of cells in S- and G2/M-phase of the cell cycle was higher in HepG2-8960-R than in HepG2. These suggest that the response of clinically relevant radioresistant (CRR) cells to fractionated radiation is not merely an accumulated response to each fractionated radiation. This is the first report on the establishment of a CRR cell line from an isogenic parental cell line. (*Cancer Sci* 2009; 100: 747–752)

Radiotherapy is one of the major therapeutic modalities for eradicating malignant tumors. The objective of radiotherapy is to achieve local control of the tumor to prevent invasion, organ failure and the seeding of secondary metastases. However, the existence of radioresistant cells remains one of the most critical obstacles in radiotherapy and radiochemotherapy. Therefore, in order to develop more effective radiotherapy we need to understand the characteristics of radioresistant cells. Since the discovery of X-rays, various efforts have been made to obtain radioresistant cells by the administration of ionizing radiation or mutagens, and molecules implicated in radioresistance are reported.[1–3] However, the concordant mechanisms of cellular radioresistance have not been clarified yet, presumably because radioresistance has been studied among cells with different genetic backgrounds, that is, cells from different origins. Published reports on genes responsible for radioresistance have analyzed surviving cells after exposure to single or several fractionated irradiations.[4,5] However, surviving cells after irradiation include many senescent-like cells which lack the ability to undergo mitosis,[6–8] suggesting that the group of cells surviving after irradiation is heterogeneous. Ionizing radiation and other genotoxic agents produce a variety of types of DNA damage. Since DNA double-strand breaks (dsbs) are considered to be the most crucial cellular damage caused by ionizing radiation, which induces cell killing, the correlation between cellular radiosensitivity and the efficiency to repair DNA dsbs has been studied in various tumor cell lines. The correlation between cellular radiosensitivity and the efficiency to repair DNA dsbs has been studied in various tumor cell lines. However, the relationship between tumor radioresistance and DNA repair capacity is still controversial.[9–11] These discrepancies are attributed to the fact that the definition of cellular radioresistance is different among different reports and that comparison is performed among cells with different genomic backgrounds. Thus, it is essential to define *in vitro* radioresistance and to establish cell lines with different radiosensitivities from a single cell line with isogenic background for elucidating the mechanisms of radioresistance.

Currently, one course of radiotherapy for tumor treatment consists of approximately 2 Gy once a day, 5 days a week, over a period of 5–8 weeks.[12] This standard fractionated exposure protocol for radiotherapy has evolved from empiric clinical experience. Therefore, we have defined *in vitro* radioresistant cells as the cells that can continue to grow even after exposure to 2 Gy/day of X-rays for more than 30 days (>60 Gy total dose). We have coined those cells clinically relevant radioresistant (CRR) cells. We established a CRR cell line, HepG2-8960-R from its parental HepG2 cell line and studied the relationship between *in vitro* radioresistance and kinetics of DNA dsbs repairs.

Micronuclei (MN) are observed in dividing cells which either contain acentric fragments and/or whole chromosomes which are unable to travel to the spindle poles during mitosis. Detection of MN provides an index of chromosome breakage and chromosome loss and is employed as a biomarker of exposure to genotoxic agents.[13] Foci of a phosphorylated histone H2AX, γ-H2AX, detected by immunofluorescence, are quantitatively the same as DNA dsbs and are capable of quantifying the repair of individual dsbs.[14] Focus formation of γ-H2AX reflects its accumulation at sites of DNA dsbs and is far more sensitive than the comet assay.[15] We report here the establishment of a CRR cell line, HepG2-8960-R and its phenotypic characteristics in induction and repair kinetics of DNA dsbs compared with its parental cell line HepG2. It is emphasized that this is the first report on the establishment of a CRR cell line toward understanding tumor radioresistance and development of more efficient radiotherapy.

Materials and Methods

Cell lines. A human hepatic carcinoma cell line, HepG2 was obtained from the Cell Resource Center for Biomedical Research, IDAC, Tohoku University, Sendai, Japan. By exposing HepG2 cells to 0.5 Gy of X-rays at every 12-h interval for more than 6 years, we obtained three long-term irradiated subcell lines. The total dose to each subcell line was more than 1600 Gy. HepG2-A was treated only by X-rays, HepG2-400 was treated once by 400 nM N-methyl-N′-nitro-N-nitrosoguanine (MNNG; Fluka Chemika Biochemika, Buchs, Switzerland) 24 h before starting

[4]To whom correspondence should be addressed.
E-mail: fukumoto@idac.tohoku.ac.jp

doi: 10.1111/j.1349-7006.2009.01082.x

long-term exposure to X-rays. HepG2-89 was exposed once to 2 Gy of α-particles by boron neutron capture before the long-term X-ray treatment. When total dose reached 1600 Gy, three subcell lines were challenged by exposure to 2 Gy of X-rays per day for 30 consecutive days. After this exposure protocol, only a few HepG2-89 cells survived while other cell lines lost their proliferative activity completely. Those surviving cells derived from HepG2-89 were cultured for another 30 days without irradiation and a subcell line HepG2-8960-R was obtained. After establishment, HepG2-8960-R cells were exposed to 2 Gy of X-rays every 24 h for more than a year. All the cells were maintained in RPMI1640 medium (Sigma-Aldrich Inc., St Louis, MO, USA) supplemented with 5% fetal bovine serum (Gibco Invitrogen Corp., Carlsbad, CA, USA) in a humidified atmosphere at 37°C with 5% CO_2 in air. For retaining characteristics influenced by long-term radiation exposure, maintenance radiation was applied to long-term exposed cells at 0.5 Gy of X-rays every 12 h and to HepG2-8960-R at 2 Gy every 24 h, respectively. Parental HepG2 cells were maintained in culture without radiation treatment for the same period as the other four subcell lines. Absence of mycoplasmas in the cell culture was periodically confirmed by a polymerase chain reaction (PCR) method.[16]

Irradiation. X-ray irradiation was performed in a 150-KVp X-ray generator (Model MBR-1520R, Hitachi, Tokyo, Japan) with a total filtration of 0.5 mm aluminum plus 0.1 mm copper filter. The dose rate was measured by a thimble ionization chamber (IC 17 A, Far West Technology, Goleta, CA, USA) at the same position as that of the samples (1.01 Gy/min). In order to investigate the effect of fractionated radiation, two X-ray exposure experiments were performed; one consisted of 2 Gy/day for 5 days, and the other was 3, 5 or 10 Gy/day for 3 days. As a control for fractionated radiation, cells with the same culture conditions except for radiation were used. All the exposure experiments in this study were performed with cells in the exponentially growing phase and 48 h after the last maintenance irradiation.

Assay for clinically relevant radioresistance. Cells (1×10^5) were seeded into a 25-cm^2 flask (Nalge Nunc International, Rochester, NY, USA) 48 h prior to the first experimental irradiation. These cells were daily exposed to 2 Gy of X-rays for 30 consecutive days. At the appropriate time point during the experiment, cells were trypsinized and single suspended cells were subcultured after the number of cells was counted. If cells continued to grow even after 30 days, these were evaluated as CRR cells.

Clonogenic assay. After a single exposure to X-rays ranging from 0 to 6 Gy, 10^3 cells were seeded into a 60-mm tissue culture dish (Becton, Dickinson and Company, Franklin Lakes, NJ, USA) coated with gelatin (Wako Pure Chemical Industries, Ltd, Osaka, Japan) and were incubated at 37°C for 10 days. After fixing with 99.5% methanol and staining with Giemsa solution (Merck & Co., Inc., Whitehouse Station, NJ, USA), colonies consisting of 50 cells or more were counted under a light microscope. Cell survival was presented as the relative ratio of colony numbers to those exposed to 2 Gy of X-rays because HepG2-8960-R cells were daily exposed to 2 Gy of X-rays for the maintenance of radioresistant characteristics.

Micronuclei. Cells (1×10^4) were seeded in 30-mm dishes (Becton, Dickinson and Co.) and treated with a fractionated exposure to 2 Gy of X-rays for 5 consecutive days. The cells were fixed with 99.5% methanol (Wako Pure Chemical Industries, Ltd, Osaka, Japan) for 10 min at room temperature (RT) and stained with Giemsa solution 24 h after irradiation. The total number of cells and cells with micronuclei was scored, respectively, under a light microscope.

Flow cytometric analysis. Exponentially growing cells were trypsinized and analyzed for the cell cycle distribution. After centrifugation for the elimination of medium, cells were washed with phosphate buffered saline (PBS), fixed with ice-cold 70% ethyl alcohol for at least 2 h and centrifuged at 210*g* for 5 min. The cell pellet was resuspended in PBS and incubated with 500 μg/mL Ribonuclease A (RNaseA) (Wako Pure Chemical Industries) at RT for 20 min, followed by staining with 50 μg/mL propidium iodide at RT for 10 min. Samples were immediately analyzed by a Cytomics FC500 (Beckman Coulter, Tokyo, Japan). In this study, aneuploid cells >2 N were less than 10% of total cells and we only examined 2 N or <2 N cells by fluorescent-activated cell sorter (FACS) analysis.

γ-H2AX foci. Cells were seeded on a cover slip 48 h before radiation exposure experiments and γ-H2AX foci were examined 24 h after the last exposure experiment to X-ray. Cells were rinsed twice with PBS and then fixed with 2% paraformaldehyde in PBS for 10 min at RT. Cells were washed twice more with PBS and permeabilized with 0.5% Triton X-100 (Wako Pure Chemical Industries, Ltd, Osaka, Japan) in PBS (PBST) for 10 min at 4°C. After two more washings with PBST, cells were blocked for 30 min in PBST with 5% skimmed milk. Anti-phosphorylated histon H2AX (γ-H2AX) primary antibody (Trevigen Inc., Gaithersburg, MD, USA) was added onto the cells. After 2-h incubation at RT, slides were washed three times with PBST for 5 min. The slides were then incubated with fluorescein isothiocyanate (FITC)-conjugated second antibody (Santa Cruz Biotechnology, Inc., Santa Cruz, CA, USA) in PBST with 5% skimmed milk for 2 h at RT. Slides were then washed three times with PBST for 5 min and were mounted with Vectashield (Vector Laboratories, Inc., Burlingame, CA, USA). γ-H2AX foci were visualized using a fluorescence microscope. Cells were judged as 'positive' for γ-H2AX if they displayed 10 or more discrete dots of brightness.[17]

Statistical analysis. At each data point, the mean and standard deviation were calculated and statistically analyzed using Student's *t*-test.

Results

Confirmation of the establishment of a radioresistant cell line with clinical relevance. HepG2 and another four subcell lines were exposed to 2 Gy of X-rays every 24 h for 30 consecutive days. Until total dose reached 20 Gy, all the cells grew well, thereafter all cells except for HepG2-8960-R ceased growing (Fig. 1a). After 30 days the cumulative dose reached 60 Gy, and all the cells

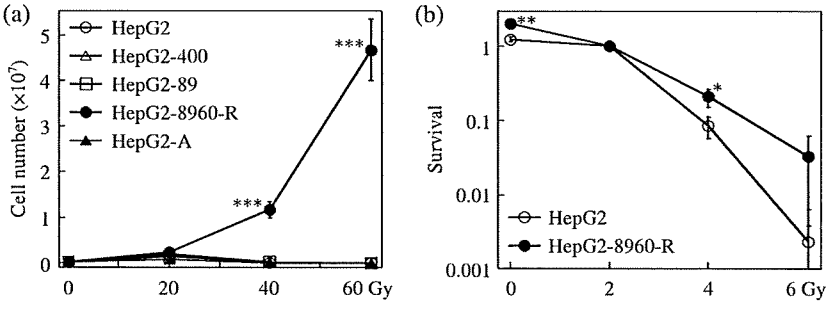

Fig. 1. Radiation sensitivity of parental HepG2 and its four subcell lines. (a) Evaluation of clinically relevant radioresistance. Exponentially growing cells were seeded 48 h before the initial irradiation. Cells were exposed to 2 Gy of X-rays every 24 h for 30 consecutive days. At the appropriate time point the total number of cells was scored. (b) Clonogenic assay. After a single exposure to X-rays at different doses, 10^3 cells were incubated for 10 days and colonies (>50 cells) were counted. Relative values of the number of colonies to that exposed to 2 Gy were calculated. Mean ± SD, $*P < 0.05$, $**P < 0.01$, $***P < 0.001$.

doi: 10.1111/j.1349-7006.2009.01082.x

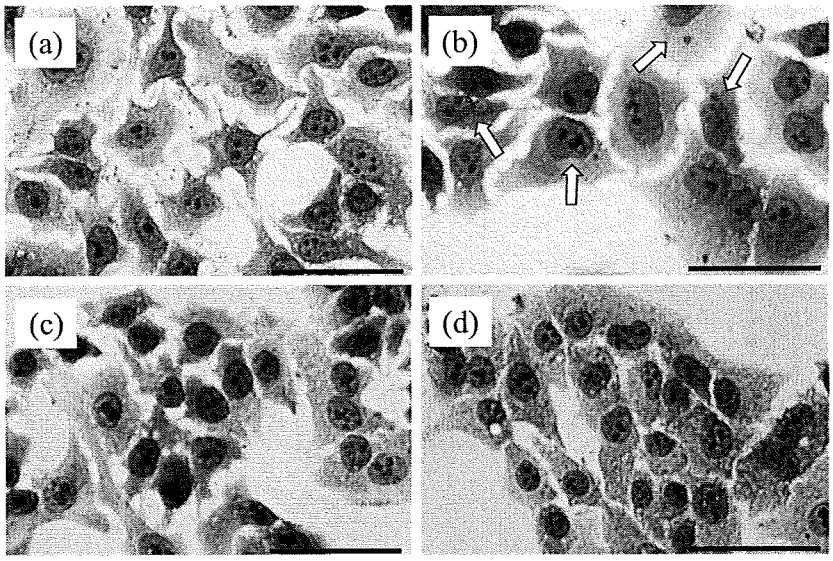

Fig. 2. Representative figures of cells with micronuclei. (a) HepG2 cells without irradiation. (b) HepG2 cells after exposure to 5 × 2 Gy of X-rays. Cells with micronuclei (white arrows) are obviously observed. (c) HepG2-8960-R cells without irradiation. (d) HepG2-8960-R cells after exposure to 5 × 2 Gy of X-rays. Scale-bar: 50 μm.

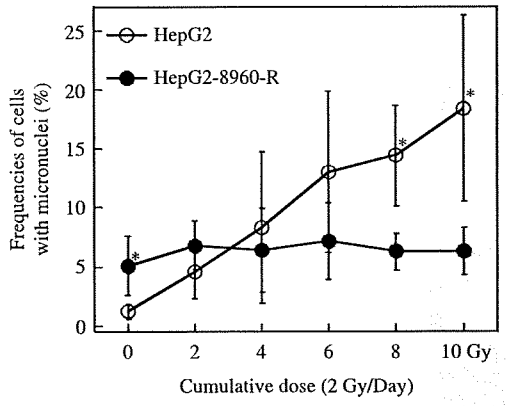

Fig. 3. Frequencies of cells with micronuclei after exposure to fractionated 2 Gy of X-rays. Mean ± SD, $*P < 0.05$.

other than HepG2-8960-R cells lost their ability to divide. The total number of HepG2-8960-R cells was 4.5×10^7 at the end of this exposure experiment after 1×10^5 cells were seeded at initiation.

Radiation sensitivity determined by clonogenic assay. HepG2-8960-R cells were radioresistant compared with parental HepG2 cells after exposure to single various doses of X-rays (Fig. 1b). Without irradiation the survival rate of HepG2-8960-R cells increased compared with cells exposed to 2 Gy and was significantly higher than that of parental HepG2 ($P < 0.05$).

Induction of micronuclei by X-ray exposure. Representative figures of cells with micronuclei are shown in Fig. 2. The effect of fractionated exposure to 2 Gy of X-rays on the formation of micronuclei is shown in Fig. 3. The basal level of HepG2-8960-R cells with micronuclei was significantly higher than that of HepG2 cells ($P < 0.05$). However, the frequency of micronuclei did not change in HepG2-8960-R cells even after exposure to 5 × 2 Gy of X-rays. In contrast, the frequency of micronuclei in HepG2 cells increased according to the cumulative dose.

The cell cycle progression after exposure to 2 Gy of X-rays. Without irradiation both the number of dead cells and the proportion of cells at S- and G2/M-phases of the cell cycle was higher in radioresistant HepG2-8960-R than in parental HepG2. The fraction of HepG2 cells at G2/M-phase increased 12 h after exposure to 2 Gy of X-rays. In contrast, G2/M fraction of HepG2-8960-R cells was constantly high and the level was the same as that of HepG2 cells 12 h after irradiation. The cell cycle distribution of HepG2 cells returned to the control level 24 h after administration of X-rays (Fig. 4).

Frequencies of cells with γ-H2AX foci after exposure to X-rays. The number of γ-H2AX foci per nucleus was less than 10 in both HepG2 and HepG2-8960-R cells without X-ray administration. Therefore, we classified cells with 10 or more than 10 γ-H2AX foci by counting 24 h after the last experimental irradiation as γ-H2AX positive cells (Fig. 5). The frequency of γ-H2AX positive HepG2 cells increased according to the cumulative dose of fractionated radiation. After exposure to 2 Gy × 5 days (total 10 Gy) of X-rays, 42.1 ± 2.7% of HepG2 cells were γ-H2AX positive while 1.2 ± 1.5% were positive before irradiation. On the other hand, the frequency of γ-H2AX positive HepG2-8960-R cells was not different before (2.2 ± 1.0%) and after exposure to total 10 Gy of X-rays (2.9 ± 0.4%) (Fig. 6a). The frequency of γ-H2AX positive cells was also determined after exposure to fractionated dose of 3, 5 and 10 Gy of X-rays for 3 consecutive days. In both HepG2 and HepG2-8960-R the frequency of γ-H2AX positive cells increased depending on the total dose. However, the frequency of γ-H2AX positive cells was significantly higher in HepG2 than in HepG2-8960-R irrespective of the total dose (Fig. 6b). After administration of 10 Gy × 3 days (total 30 Gy) of X-rays, all HepG2 cells were positive for γ-H2AX with increase of nuclear size (Figs 5b and 6b). On the other hand, approximately 30% of HepG2-8960-R cells were negative for γ-H2AX after exposure to 10 Gy × 3 days (Figs 5d and 6b).

Discussion

It is not so difficult to obtain radiosensitive cells by the administration of genotoxic stresses or the knockdown technique of some genes.[18–22] However, there is no report dealing with the establishment of CRR cell lines. To establish anticancer drug-resistant cell lines, cells are continuously exposed to cytotoxic reagents and are usually selected by the stepwise increase of the drug concentration. By this process, many drug-resistant cells have been obtained and used to elucidate the mechanisms of drug resistance.[23] However, our preliminary experiments revealed that a simple stepwise increase of dose was not applicable for the selection of CRR cells. The selecting condition of irradiation

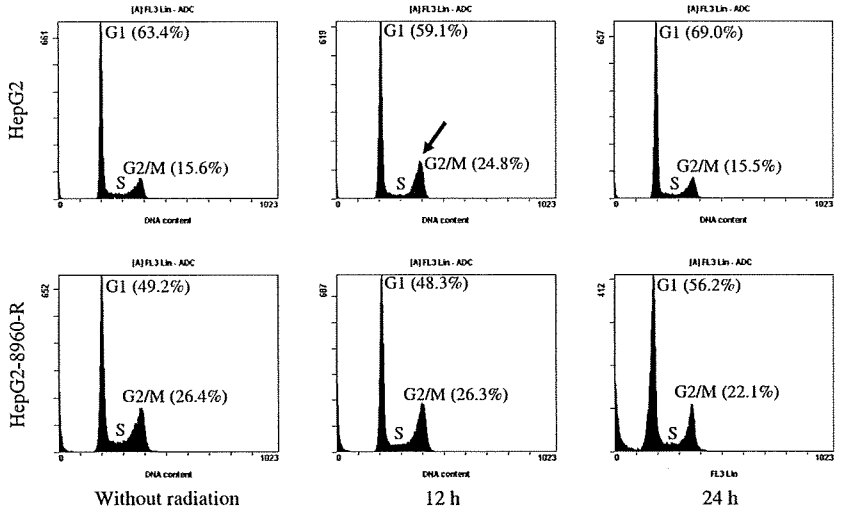

Fig. 4. Flow cytometric analysis of cell cycle distribution 12 and 24 h after a single exposure to 2 Gy of X-rays. In HepG2 cells increased G2/M arrest was apparently observed 12 h after irradiation (arrow), whereas the level of G2/M was constantly high in HepG2-8960-R cells.

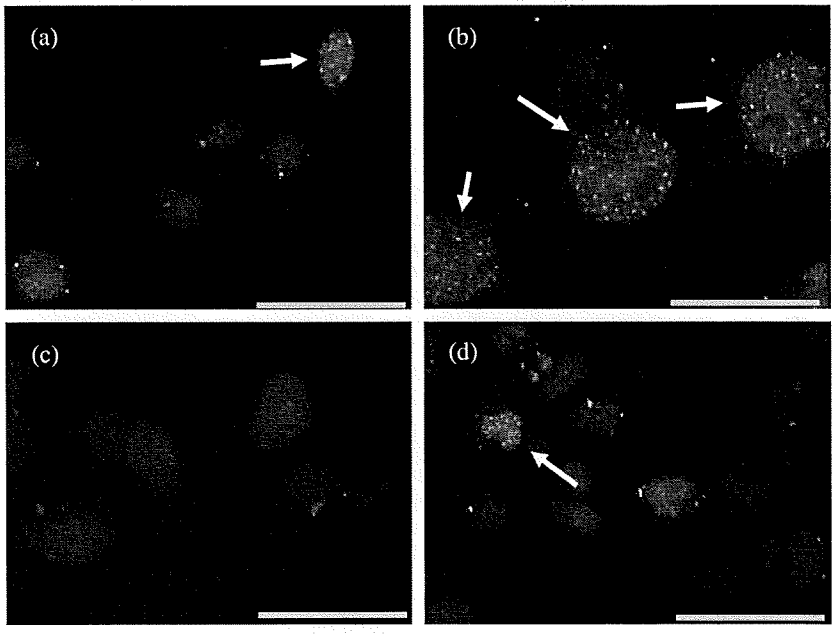

Fig. 5. Immunofluorescent staining of γ-H2AX foci. HepG2 (a) and HepG2-8960-R (c) cells without irradiation. HepG2 (b) and HepG2-8960-R cells (d) 24 h after exposure to 10 × 3 Gy of X-rays. All the HepG2 cells possessed 10 or more γ-H2AX foci. It is noted that the nuclear size of HepG2 cells increased after irradiation. Arrows indicate the cells with 10 or more γ-H2AX foci. Scale-bar: 50 μm.

is antinomic: whether the period of acute exposure should be extremely short compared with the cell cycle period, or exposure dose rate should be extremely low if continuous irradiation is applied. Recently, cellular radioresistance has been widely investigated for the development of more effective tumor radiotherapy or the identification of clinical markers to predict tumor radiosensitivity.[24–28] In those investigations, cellular radiosensitivity was usually determined by clonogenic assay,[29] or other cell proliferation assays such as the methylthiotetrazole (MTT) assay.[30] A course of conventional radiotherapy is composed of 2 Gy a day, 5 days a week over a period of 4–6 weeks. Therefore, in order to understand the molecular mechanisms of radioresistance under tumor radiotherapy, we need to investigate cells *in vitro* that can proliferate with daily exposure to 2 Gy of X-rays for at least 30 days, that is, CRR cells.

The correlation between tumor radioresistance and the efficiency of DNA dsbs repair is a matter of controversy. Radioresistant cells show more efficient initial rejoining of DNA dsbs than radiosensitive cells *in vitro* after irradiation determined by the comet assay.[9] The same assay revealed no correlation between tumor radiosensitivity and DNA dsbs induction or rejoining.[10,31] The rate of DNA dsbs repair is a critical factor underlying radioresistance in human tumor cell lines determined by DNA elution analysis.[32] Radiosensitive tumor cells and their xenografts retain γ-H2AX for a greater duration than radioresistant cells and tumors after irradiation,[17] and the rate of disappearance of γ-H2AX foci during the first few hours after irradiation is faster in more radioresistant cells than in less resistant cells.[33] On the contrary, measurements of immunofluorescence intensity of γ-H2AX are not able to reliably rank cells according to their clonogenic survival after irradiation.[34] These inconsistent results are due to the different definitions of cellular radioresistance and the usage of cells with different genomic backgrounds. To overcome these problems we established a CRR cell line, HepG2-8960-R, from isogenic parental HepG2.

It is known that there are two DNA dsbs repair pathways, the non-homologous end joining pathway (NHEJ) and the homologous recombination pathway (HR).[35] NHEJ precedes HR and NHEJ

doi: 10.1111/j.1349-7006.2009.01082.x

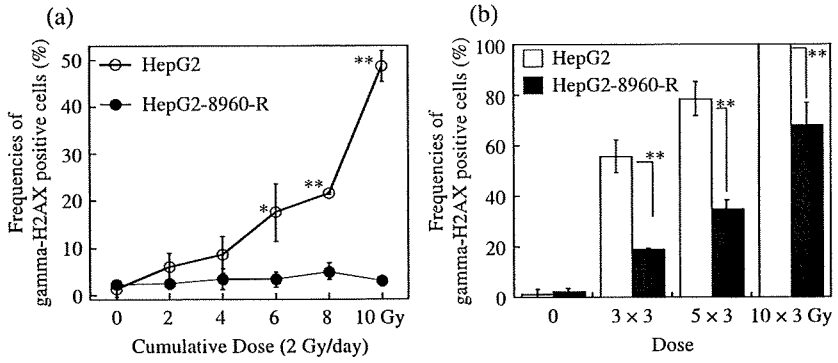

Fig. 6. Frequencies of γ-H2AX positive cells after exposure to fractionated X-rays. γ-H2AX foci were counted 24 h after the last experimental exposure to X-rays. Each fraction consisted of 2 Gy (a), and 3, 5 and 10 Gy (b). Mean ± SD $*P < 0.05$, $**P < 0.01$.

can, in principle, repair dsbs with a different degree of fidelity, while HR removes DNA dsbs by utilizing homologous DNA segments and restores faithfully the original DNA sequence around the break.[36–38] Akudugu *et al.* demonstrated that radioresistance evaluated by clonogenic assay is positively correlated to MN yield in a panel of cell lines.[39] These suggest that fast DNA dsbs rejoining mediated by NHEJ, possibly moderated by the slow HR, plays a major role in MN formation and total DNA dsbs rejoining influences cell survival. In the present study, the frequency of MN in Hep G2-8960-R at the basal level was higher than that in Hep G2, however, the frequency of MN in Hep G2-8960-R induced by fractionated radiation was lower than that in Hep G2. The frequency of spontaneous MN in lymphocytes from radiation workers is more than nonexposed individuals; however, MN frequency is lower for radiation workers after 1 and 2-Gy of *in vitro* radiation.[40] Although a fraction of 2 Gy is higher than the usual preconditioning dose for adaptive response, the current study suggests that radioresistance with clinical relevance is a kind of adaptive response. Interestingly, no correlation between the level of strand breaks as measured by the comet assay and the γ-H2AX signal is reported in blood cells exposed to a DNA dsbs-inducing drug.[41] All these suggest that the response of CRR cells to fractionated radiation is not merely an accumulated response to each fractionated radiation. It is essential to analyze the molecular mechanisms of radiation responses in CRR cells for conquering radioresistance of malignant tumors, particularly in relation to NHEJ and HR.

The number of dead cells was higher in HepG2-8960-R than in HepG2, indicating that the cells receiving fatal hits after cumulative fractionated radiation are always eliminated from the proliferating cell population of HepG2-8960-R. The fraction of S-G2/M-phase of HepG2-8960-R was higher than that of HepG2. HR is the most active in late-S- and G2-phases of the cell cycle.[42,43] Moreover, by every 24-h administration of fractionated 3, 5 and 10 Gy of X-rays for 3 days, the frequency of γ-H2AX positive cells was lower in HepG2-8960-R than that in HepG2. These results strongly suggest that DNA dsbs induced by fractionated radiation were rejoined more efficiently and more accurately in radioresistant HepG2-8960-R than in parental HepG2. These results also suggest that the contribution of HR pathway to repair X-ray-induced dsbs in HepG2-8960-R cells is higher than that in HepG2 cells. However, further study is needed to draw a conclusion. The reason why HepG2-8960-R cells tolerated clinically relevant doses of X-rays could be partly attributed to the increase of the S-phase fraction because radioresistance is the highest in the S-phase.[44] Accumulation of S-G2/M-phase of HepG2-8960-R was observed after exposure to 5 Gy of X-rays (data not shown). The dose rate, 2 Gy/day used in radiotherapy, may have a particular meaning, although this has been determined empirically.

Endoreduplication of p53 mutant cells during G2 arrest is associated with radioresistance.[45] Our preliminary Comparative Genomic Hybridization (CGH) and chromosome analysis revealed chromosomal stability in HepG2-8960-R with wild-type p53 (data not shown). These are different from the notion that ionizing radiation induces genomic instability.[46] Among four long-term irradiated cell lines in this study, HepG2-A cells were stably hyperploid without CRR characteristics. These suggest that formation of endopolyploid cells is not associated with a CRR trait. It would be interesting to elucidate if the mechanism, which reciprocally regulates roles of NHEJ and HR, exists or not in relation to CRR phenotype.

We emphasize that this is the first report on the establishment of a CRR cell line from an isogenic parental cell line. The combination of HepG2 and HepG2-8960-R is the most suitable tool to understand acquired radioresistance under radiotherapy and to develop more effective radiotherapy. We are now underway to analyze molecules involved in DNA dsbs repair and gene expression profile of HepG2-8960-R cells in comparison with parental HepG2 cells.

Acknowledgments

This study was supported in part by the Grants-in Aid from the Ministry of Education, Science, Sports and Culture and the Ministry of Health, Labour and Welfare of Japan.

References

1 Deschavanne PJ, Fertil B. A review of human cell radiosensitivity *in vitro*. *Int J Radiat Oncol Biol Phys* 1996; **34**: 251–66.
2 Jameel JK, Rao VS, Cawkwell L, Drew PJ. Radioresistance in carcinoma of the breast. *Breast* 2004; **13**: 452–60.
3 Tanio Y, Watanabe M, Inoue T *et al.* Chemo-radioresistance of small cell lung cancer cell lines derived from untreated primary tumors obtained by diagnostic bronchofiberscopy. *Jpn J Cancer Res* 1990; **81**: 289–97.
4 Tang WY, Chau SP, Tsang WP, Kong SK, Kwok TT. The role of Raf-1 in radiation resistance of human hepatocellular carcinoma HepG2 cells. *Oncol Rep* 2004; **12**: 1349–54.
5 Wei K, Kodym R, Jin C. Radioresistant cell strain of human fibrosarcoma cells obtained after long-term exposure to X-rays. *Radiat Environ Biophys* 1998; **37**: 133–7.
6 Mirzayans R, Scott A, Cameron M, Murray D. Induction of accelerated senescence by gamma radiation in human solid tumor-derived cell lines expressing wild-type TP53. *Radiat Res* 2005; **163**: 53–62.
7 Oh CW, Bump EA, Kim JS, Janigro D, Mayberg MR. Induction of a senescence-like phenotype in bovine aortic endothelial cells by ionizing radiation. *Radiat Res* 2001; **156**: 232–40.
8 Suzuki K, Mori I, Nakayama Y, Miyakoda M, Kodama S, Watanabe M. Radiation-induced senescence-like growth arrest requires TP53 function but not telomere shortening. *Radiat Res* 2001; **155**: 248–53.
9 Bergqvist M, Brattstrom D, Stalberg M, Vaghef H, Brodin O, Hellman B. Evaluation of radiation-induced DNA damage and DNA repair in human lung cancer cell lines with different radiosensitivity using alkaline and neutral single cell gel electrophoresis. *Cancer Lett* 1998; **133**: 9–18.
10 Olive PL, Banath JP, MacPhail HS. Lack of a correlation between radiosensitivity and DNA double-strand break induction or rejoining in six human tumor cell lines. *Cancer Res* 1994; **54**: 3939–46.
11 Sakata K, Someya M, Matsumoto Y, Hareyama M. Ability to repair DNA

double-strand breaks related to cancer susceptibility and radiosensitivity. *Radiat Med* 2007; **25**: 433–8.
12 Tannock I. *The Basic Science of Oncology*, 4th edn. New York: McGraw-Hill, Medical Publications, 2005.
13 Fenech M. The in vitro micronucleus technique. *Mutat Res* 2000; **455**: 81–95.
14 Rothkamm K, Lobrich M. Evidence for a lack of DNA double-strand break repair in human cells exposed to very low x-ray doses. *Proc Natl Acad Sci USA* 2003; **100**: 5057–62.
15 Clingen PH, Wu JY, Miller J *et al.* Histone H2AX phosphorylation as a molecular pharmacological marker for DNA interstrand crosslink cancer chemotherapy. *Biochem Pharmacol* 2008; **76**: 19–27.
16 Harasawa R, Mizusawa H, Nozawa K, Nakagawa T, Asada K, Kato I. Detection and tentative identification of dominant mycoplasma species in cell cultures by restriction analysis of the 16S-23S rRNA intergenic spacer regions. *Res Microbiol* 1993; **144**: 489–93.
17 Taneja N, Davis M, Choy JS *et al.* Histone H2AX phosphorylation as a predictor of radiosensitivity and target for radiotherapy. *J Biol Chem* 2004; **279**: 2273–80.
18 Iwasaki I, Sugiyama H, Kanazawa S, Hemmi H. Establishment of cisplatin-resistant variants of human neuroblastoma cell lines, TGW and GOTO, and their drug cross-resistance profiles. *Cancer Chemother Pharmacol* 2002; **49**: 438–44.
19 Landmark H, Nahas SA, Aaroe J, Gatti R, Borresen-Dale AL, Rodningen OK. Transcriptional response to ionizing radiation in human radiation sensitive cell lines. *Radiother Oncol* 2007; **83**: 256–60.
20 Saga Y, Suzuki M, Machida S, Ohwada M, Sato I. Establishment of a new cell line (TAYA) of clear cell adenocarcinoma of the ovary and its radiosensitivity. *Oncology* 2002; **62**: 180–4.
21 Slijepcevic P. Is there a link between telomere maintenance and radiosensitivity? *Radiat Res* 2004; **161**: 82–6.
22 Uchiyama-Kokubu N, Watanabe T. Establishment and characterization of adriamycin-resistant human colorectal adenocarcinoma HCT-15 cell lines with multidrug resistance. *Anticancer Drugs* 2001; **12**: 769–79.
23 Hait WNE. *Drug Resistance (Cancer Treatment and Research)*. Holland, Springer Verl.: Kluwer Academic Pub, 1996.
24 An J, Chervin AS, Nie A, Ducoff HS, Huang Z. Overcoming the radioresistance of prostate cancer cells with a novel Bcl-2 inhibitor. *Oncogene* 2007; **26**: 652–61.
25 Bao S, Wu Q, McLendon RE *et al.* Glioma stem cells promote radioresistance by preferential activation of the DNA damage response. *Nature* 2006; **444**: 756–60.
26 Lee HC, Kim DW, Jung KY *et al.* Increased expression of antioxidant enzymes in radioresistant variant from U251 human glioblastoma cell line. *Int J Mol Med* 2004; **13**: 883–7.
27 Wang T, Tamae D, LeBon T, Shively JE, Yen Y, Li JJ. The role of peroxiredoxin II in radiation-resistant MCF-7 breast cancer cells. *Cancer Res* 2005; **65**: 10338–46.
28 Weichselbaum RR, Beckett MA, Hallahan DE, Kufe DW, Vokes EE. Molecular targets to overcome radioresistance. *Semin Oncol* 1992; **19**: 14–20.
29 Puck TT, Marcus PI. Action of x-rays on mammalian cells. *J Exp Med* 1956; **103**: 653–66.
30 Vistica DT, Skehan P, Scudiero D, Monks A, Pittman A, Boyd MR. Tetrazolium-based assays for cellular viability: a critical examination of selected parameters affecting formazan production. *Cancer Res* 1991; **51**: 2515–20.
31 Hellman B, Brodin D, Andersson M *et al.* Radiation-induced DNA-damage and gene expression profiles in human lung cancer cells with different radiosensitivity. *Exp Oncol* 2005; **27**: 102–7.
32 Schwartz JL, Rotmensch J, Giovanazzi S, Cohen MB, Weichselbaum RR. Faster repair of DNA double-strand breaks in radioresistant human tumor cells. *Int J Radiat Oncol Biol Phys* 1988; **15**: 907–12.
33 Olive PL, Banath JP. Phosphorylation of histone H2AX as a measure of radiosensitivity. *Int J Radiat Oncol Biol Phys* 2004; **58**: 331–5.
34 Mahrhofer H, Burger S, Oppitz U, Flentje M, Djuzenova CS. Radiation induced DNA damage and damage repair in human tumor and fibroblast cell lines assessed by histone H2AX phosphorylation. *Int J Radiat Oncol Biol Phys* 2006; **64**: 573–80.
35 Shrivastav M, De Haro LP, Nickoloff JA. Regulation of DNA double-strand break repair pathway choice. *Cell Res* 2008; **18**: 134–47.
36 Delacote F, Han M, Stamato TD, Jasin M, Lopez BS. An xrcc4 defect or Wortmannin stimulates homologous recombination specifically induced by double-strand breaks in mammalian cells. *Nucl Acids Res* 2002; **30**: 3454–63.
37 Frank-Vaillant M, Marcand S. Transient stability of DNA ends allows nonhomologous end joining to precede homologous recombination. *Mol Cell* 2002; **10**: 1189–99.
38 Kim JS, Krasieva TB, Kurumizaka H, Chen DJ, Taylor AM, Yokomori K. Independent and sequential recruitment of NHEJ and HR factors to DNA damage sites in mammalian cells. *J Cell Biol* 2005; **170**: 341–7.
39 Akudugu JM, Slabbert JP, Serafin A, Bohm L. Frequency of radiation-induced micronuclei in neuronal cells does not correlate with clonogenic survival. *Radiat Res* 2000; **153**: 62–7.
40 Gourabi H, Mozdarani H. A cytokinesis-blocked micronucleus study of the radioadaptive response of lymphocytes of individuals occupationally exposed to chronic doses of radiation. *Mutagenesis* 1998; **13**: 475–80.
41 Ismail IH, Wadhra TI, Hammarsten O. An optimized method for detecting gamma-H2AX in blood cells reveals a significant interindividual variation in the gamma-H2AX response among humans. *Nucleic acids Res* 2007; **35**: e36.
42 Hendrickson EA. Cell-cycle regulation of mammalian DNA double-strand-break repair. *Am J Hum Genet* 1997; **61**: 795–800.
43 Rothkamm K, Kruger I, Thompson LH, Lobrich M. Pathways of DNA double-strand break repair during the mammalian cell cycle. *Mol Cell Biol* 2003; **23**: 5706–15.
44 Hall EJ, Giaccia AJ. *Radiobiology for the Radiologist*, 6th edn. Philadelphia, London: Lippincott Williams & Wilkins, 2006.
45 Ivanov A, Cragg MS, Erenpreisa J, Emzinsh D, Lukman H, Illidge TM. Endopolyploid cells produced after severe genotoxic damage have the potential to repair DNA double strand breaks. *J Cell Sci* 2003; **116**: 4095–106.
46 Mothersill C, Seymour C. Lethal mutations and genomic instability. *Int J Radiat Biol* 1997; **71**: 751–8.

doi: 10.1111/j.1349-7006.2009.01082.x

FEBS Letters 582 (2008) 2431–2434

Crucial role of peroxiredoxin III in placental antioxidant defense of mice

Lianqin Li[a,b,*], Wataru Shoji[a], Hiroaki Oshima[a], Masuo Obinata[a], Manabu Fukumoto[c], Naoko Kanno[c]

[a] *Department of Cell Biology, Institute of Development, Aging, and Cancer, Tohoku University, Sendai 980-8575, Japan*
[b] *Department of Obstetrics and Gynecology, Peking University First Hospital, 1 Xi'anmen Dajie, Xicheng District, Beijing 100034, China*
[c] *Department of Pathology, Institute of Development, Aging, and Cancer, Tohoku University, Sendai 980-8575, Japan*

Received 28 May 2008; accepted 30 May 2008

Available online 9 June 2008

Edited by Barry Halliwell

Abstract **We observed frequent stillbirth in peroxiredoxin III (PrxIII) knockout maternal mice. Quantitative real time PCR (qRT-PCR) and Western-blot analysis revealed increased oxidative stress in placentas that were deficient in PrxIII. We did not find significant difference between PrxIII knockout maternal mice and wild-type littermates in hematological parameters, fetal number, and embryonic development. Nevertheless, we noticed enhanced expression of PrxI in erythrocytes of pregnant knockout mice. Our results provided in vivo evidence that PrxIII played a crucial role in placental antioxidant defense. Up-regulation of PrxI might provide a compensation that protected erythrocytes against oxidative damage.**

Keywords: Stillbirth; Peroxiredoxin III (PrxIII); Placenta; Oxidative stress

1. Introduction

As a member of peroxiredoxin (Prx) family, PrxIII was predominantly localized in mitochondria and was considered to play an important role in mitochondrial antioxidant defense [1–3]. Mammalian PrxIII has two active cysteines that reduce H_2O_2 with the use of electrons provided by thioredoxin [4]. Recently, we studied in vivo function of PrxIII using PrxIII knockout (PrxIII−/−) mice. Severe lung inflammation and oxidized DNA/protein in alveolar epithelium were detected in PrxIII−/− mice exposed to intratracheal inoculation of lipopolysaccharide (LPS), indicating that PrxIII was an indispensable scavenger of reactive oxygen species (ROS) in mouse lungs under oxidative stress [5].

During the preparation of experimental mice, we observed frequent stillbirth in PrxIII−/− maternal mice. Since PrxIII was previously suggested to play an important role in placenta under oxidative stress [6,7], we were interested in analyzing in vivo function of PrxIII in pregnancy. According to previous studies, oxidative stress was relatively high in pregnancy and was further increased during labor [8,9]. On the other hand, antioxidant activity was accordingly increased with gestational progression to protect against oxidative damage [10,11]. Abundance of ROS or decrease of antioxidant activity would disturb oxidative balance and ultimately result in pathological changes. For example, a pregnant complication in human beings called pre-eclampsia was related to oxidative stress [12].

In the present study, we compared pregnant outcomes between PrxIII−/− maternal mice and wild-type (PrxIII+/+) littermates. We also investigated hematological parameters, fetal number, embryonic development, and placental oxidative stress in maternal mice.

2. Materials and methods

2.1. Mouse mating

PrxIII−/− mice were generated as described before [5]. We mated C57BL/6 (B6) mice with PrxIII−/− mice to generate PrxIII+/− offspring. The offspring were then intercrossed to produce PrxIII+/+, PrxIII+/−, and PrxIII−/− littermates for experiments.

2.2. Hematological examination on peripheral blood and histological inspection on placentas

Peripheral blood was examined on mice before pregnancy and at the 18th day of pregnancy. Hematological parameters included erythrocyte count, reticulocyte count, and hematocrit. In addition, existence of Heinz body in erythrocytes was examined on smears stained with brilliant cresyl blue.

Placentas were removed from maternal mice that were pregnant for 18 days. Two pathologists without knowledge of PrxIII genotypes examined placental sections after HE-staining.

2.3. Analysis of oxidative state in placentas

Eighteen-day placentas were homogenized and protein concentration was detected by Bio-Rad protein assay kit. After separation on 15% SDS–PAGE and transfer to Immobilon membrane (Millipore Corporation), lipid oxidation was estimated with anti-4-hydroxy-2-nonenal (4-HNE) monoclonal antibody (Japan Institute for Control of Aging, Fukuroi, Japan). Visualization was achieved with ECL Western-blotting detection system (Amersham). Anti-β-actin antibody (Sigma) was used as internal control.

In a separate experiment, RNA samples were prepared from placentas. After synthesis of first-strand cDNA, quantitative real time PCR (qRT-PCR) was performed to analyze expressions of prepro-endothelin 1 (prepro-ET-1) and tumor necrosis factor alpha (TNF-α). Primer sequences are indicated in Table 1. β-Actin was used as internal control. SYBR® GreenER™ Two-step qRT-PCR Kits was purchased from Invitrogen. qRT-PCR was performed on Bio-Rad iCycler by the following program: 95 °C 3 min, (95 °C 15 s, 60 °C

*Corresponding author. Address: Department of Obstetrics and Gynecology, Peking University First Hospital, 1 Xi'anmen Dajie, Xicheng District, Beijing 100034, China. Fax: +86 10 88257362.
E-mail address: lilq2005@126.com (L. Li).

Abbreviations: Prx, peroxiredoxin; qRT-PCR, quantitative real time polymerase chain reaction; LPS, lipopolysaccharide; ROS, reactive oxygen species; 4-HNE, 4-hydroxy-2-nonenal; Prepro-ET-1, prepro-endothelin 1; TNF-α, tumor necrosis factor alpha; PBS, phosphate-buffered saline

0014-5793/$34.00
doi:10.1016/j.febslet.2008.05.050

Table 1
Primer sequences for qRT-PCR analysis

Genes	Forward	Reverse
prepro-ET-1	5′-CTGGACATCATCTGGGTCAA-3′	5′-CTGCTTGGCAGAAATTCCA-3′
TNF-α	5′-GATTATGGCTCAGGGTCCAA-3′	5′-CCCATTTGAGTCCTTGATGG-3′
PrxI	5′-CTGCCAAGTGATTGGTGCTT-3′	5′-CCCATAATCCTGAGCAATGGT-3′
PrxII	5′-AGATCATCGCGTTCAGCAAC-3′	5′-CAAGCGTCTGGTCACGTCAG-3′
PrxIII	5′-CAGCCGTTGTCAATGGAGAG-3′	5′-TCACATCGTGAAATTCGTTAGC-3′
β-Actin	5′-ACGTTGACATCCGAAAGACC-3′	5′-CCACCGATCCACACAGAGTA-3′

60 s) × 40. Reaction volume was 50 μl. Expression of oxidative makers was calculated by equation $2^{-\Delta Ct} \times 10^6$, where $\Delta Ct = [Ct_{prepro\text{-}ET\text{-}1}$ (or $Ct_{TNF\text{-}\alpha}) - Ct_{\beta\text{-}actin}]$. Three separate reactions were performed for each gene.

2.4. Analysis of PrxI, PrxII, and PrxIII expression in erythrocytes

Total blood (about 1 ml) was obtained from mice that were pregnant for 18 days. Red blood cells were isolated with Ficoll-Paque (Pharmacia Biotech) and washed two times with phosphate-buffered saline (PBS). RNA and cell lysates were, respectively, prepared from isolated erythrocytes. Expression of PrxI, PrxII, and PrxIII was detected by qRT-PCR and Western blot. Primer sequences for qRT-PCR are indicated in Table 1. For Western-blot analysis, we used rabbit anti-PrxIII serum immunized with PrxIII C-terminal oligopeptide [5].

2.5. Statistic analysis

For qRT-PCR results, relative expression of detected genes was compared among PrxIII+/+, PrxIII+/−, and PrxIII−/− samples by analysis of variance. $P < 0.05$ was considered to be statistically significant.

3. Results

3.1. Breeding abnormality in PrxIII−/− maternal mice

After successful generation of PrxIII−/− mice, we mated PrxIII−/− mice with wild-type (B6) ones to produce heterozygous offspring (PrxIII+/−), which were intended to intercross to generate PrxIII+/+, PrxIII+/−, and PrxIII−/− littermates for experiment. Unexpectedly, we noticed that live newborns from individual PrxIII−/− maternal mouse were only 1–3, or even zero (mean litter size: 1.2 ± 0.5, $n = 6$), while B6 maternal mice gave birth to 5–8 live newborns (mean litter size: 6.7 ± 0.5, $n = 6$).

To confirm our observation, we mated PrxIII+/+ and PrxIII−/− male mice with PrxIII+/+, PrxIII+/− and PrxIII−/− female littermates, respectively. Offspring number from PrxIII−/− maternal mice (mean litter size: 0.8 ± 0.3, $n = 6$) was much smaller than that from PrxIII+/+ (mean litter size: 7.5 ± 0.3, $n = 6$) and PrxIII+/− (mean litter size: 7.2 ± 0.2, $n = 6$) maternal littermates. Therefore, pregnant outcome was only related to genotypes of female mice. We then closely monitored maternal mice around delivery time and found that newborns were already dead at birth.

To understand fetal features before delivery, we killed pregnant mice on the 18th day of second gestation and found that fetuses in PrxIII−/− maternal mice were still alive. The mean fetal numbers were 7.3 ± 0.7 for PrxIII+/+, 7.3 ± 0.5 for PrxIII+/−, and 7.0 ± 0.8 for PrxIII−/− maternal mice, while the mean fetal weights were 1.442 ± 0.072 g ($n = 44$), 1.326 ± 0.09 g ($n = 44$), and 1.285 ± 0.065 g ($n = 42$), respectively. There was no difference in fetal number or fetal weight among maternal mice with different genotypes.

3.2. Hematological parameters and placental histology

Hematological parameters were not different among PrxIII+/+, PrxIII+/−, and PrxIII−/− mice (Table 2), and no Heinz body was observed in erythrocytes (data not shown). In detail, both erythrocyte count and hematocrit in peripheral blood were decreased after pregnancy, especially in PrxIII−/− maternal mice, although the decrease did not reach statistical significance ($P > 0.05$). Reticulocyte count was significantly increased in pregnant mice ($P < 0.05$).

As shown in Fig. 1, focal necrosis and hyaline degeneration in trophoblast giant cells (black arrows) and degeneration in vessel walls (white arrows) were observed in placentas that were derived from PrxIII−/− maternal mice.

3.3. Increased oxidative stress in placentas of PrxIII−/− maternal mice

To further understand pathological changes related to fetal death, we examined oxidative states in placentas. As an α,β-unsaturated aldehyde derived from peroxidation of ω6-unsaturated fatty acids, 4-HNE can efficiently react with sulfhydryl groups or histidine and lysine groups of proteins to form stable 4-HNE-protein compound, which is specifically recognized by anti 4-HNE antibody [13]. As shown in Fig. 2, high level of 4-HNE-modified protein was detected in placenta of Prx III−/− maternal mice as compared with PrxIII+/+ or PrxIII+/− samples. In addition, qRT-PCR analysis revealed that expressions of prepro-ET-1 and TNF-α were 6.24- and 2.66-fold higher, respectively, in PrxIII−/− placenta than in PrxIII+/+ placenta (Fig. 3). There was no significant difference in prepro-ET-1 or TNF-α expression between PrxIII+/+ and PrxIII+/− placentas.

Table 2
Hematological parameters in mice before and after pregnancy (means ± S.E.)

Genotype ($n = 6$)	Erythrocyte (10^6/μl)		Reticulocyte (%)		Hematocrit (%)	
PrxIII+/+	9.0 ± 0.4	7.8 ± 0.3	1.3 ± 0.5	5.6 ± 1.1*	50 ± 1.8	45 ± 0.7
PrxIII+/−	8.8 ± 0.2	7.5 ± 0.2	1.3 ± 0.6	5.4 ± 0.8*	50.3 ± 2.4	44.2 ± 1.6
PrxIII−/−	8.7 ± 0.2	6.5 ± 0.3	1.4 ± 0.4	4.9 ± 1.0*	49.6 ± 0.3	40.5 ± 0.4

There was no significant difference in hematological parameters among non-pregnant mice. Erythrocyte count and hematocrit became relatively low after pregnancy, especially in PrxIII−/− maternal mice. The percentage of reticulocytes was significantly increased in pregnant mice (*$P < 0.05$). Left number: before pregnancy and right number: after pregnancy.

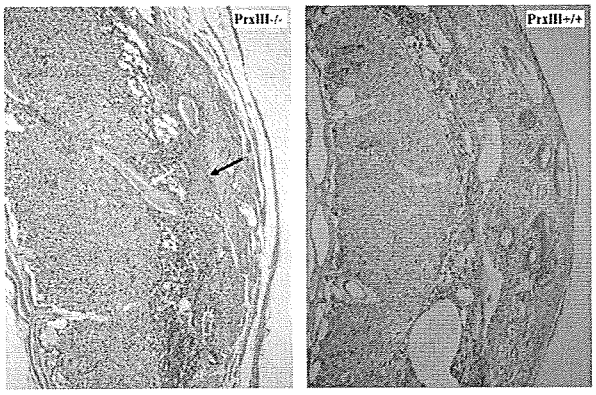

Fig. 1. Histological examination on HE-stained placental sections. Focal necrosis and hyaline degeneration in trophoblast giant cells (black arrows) and degeneration in vessel walls (white arrows) were observed in placentas derived from PrxIII−/− maternal mice. Original magnification: ×40.

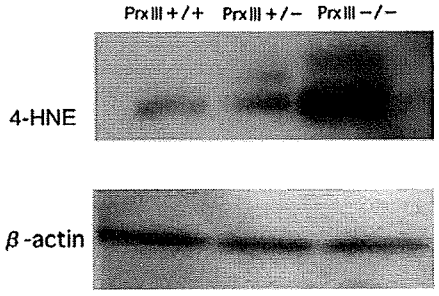

Fig. 2. Western-blot analysis for 4-HNE-modified protein in placental tissues. A signal with 51 kDa molecular size was significantly enhanced in PrxIII−/− placenta.

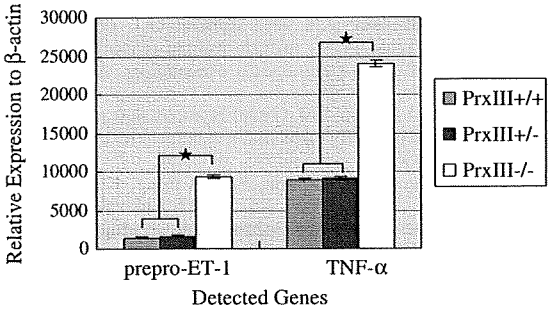

Fig. 3. Representative results of qRT-PCR for placental prepro-ET-1 and TNF-α expressions. Both prepro-ET-1 and TNF-α were significantly up-regulated in PrxIII−/− placenta as compared with PrxIII+/+ and PrxIII+/− samples (PrxIII−/− vs. PrxIII+/+ and PrxIII+/−: $^{\star}P < 0.01$).

3.4. Expression of PrxI, PrxII, and PrxIII in erythrocytes of pregnant mice

As indicated in Fig. 4, PrxIII protein was undetectable in erythrocytes of PrxIII−/− mice. However, we noticed an extra 28-kDa signal that was most enhanced in PrxIII−/− sample. Since PrxIII oligopeptide used to raise anti-PrxIII antibody shares more than 56% amino acid sequences with PrxI and PrxII C-terminals [5], the antibody might has cross-reactivity

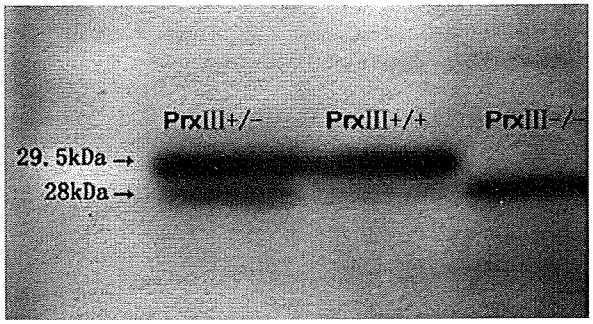

Fig. 4. Western-blot analysis for PrxIII expression in mouse erythrocytes. An extra 28 kDa signal was observed and was most enhanced in PrxIII−/− sample that was deficient in PrxIII protein.

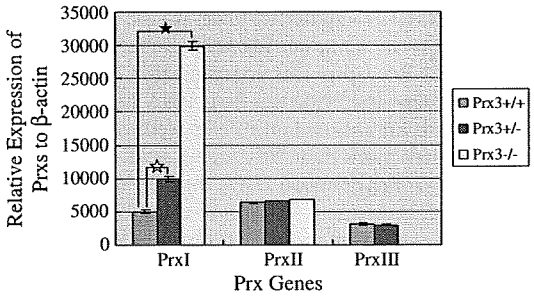

Fig. 5. Representative results of qRT-PCR for Prx expression in erythrocytes of pregnant mice. PrxI mRNA was predominantly increased in erythrocytes of PrxIII−/− and PrxIII+/− mice as compared with PrxIII+/+ littermates (PrxIII−/− vs. PrxIII+/+: $^{\star}P < 0.01$; PrxIII+/− vs. PrxIII+/+: $^{\star}P < 0.05$).

with PrxI and PrxII proteins. We supposed that the extra band represented PrxI protein as the molecular size of the signal corresponded to PrxI molecular weight. To confirm our hypothesis, we performed qRT-PCR analysis to detect mRNA of PrxI, PrxII, and PrxIII in erythrocytes of pregnant mice. The results revealed that PrxI was predominantly up-regulated by 6-fold in PrxIII−/− mice and 2-fold in PrxIII+/− mice as compared with that in PrxIII+/+ littermates (Fig. 5). We did not find significant change of Prx II expression.

4. Discussion

In the present study, we demonstrated frequent stillbirth and serious placental oxidation in PrxIII−/− maternal mice. Since fetal fates were dependent on the phenotypes of maternal mice instead of that of fetuses themselves, we suggested that mechanism of fetal death in PrxIII−/− maternal mice might be due to the functional lack of PrxIII in placenta.

In addition to placental vessel lesions, lipid oxidation was significantly increased in placentas from PrxIII−/− maternal mice. According to previous reports, oxidative stress could induce expressions of TNF-α and endothelin-1 [14–16]. Elevated level of TNF-α in PrxIII−/− mouse placentas further demonstrated increased placental oxidative stress. More importantly, high expression of placental prepro-ET-1 suggested excessive production of mature endothelin-1, which would cause vascular spasm and subsequent low blood supply in placenta. Low

blood supply, together with oxidative damage in placenta, would result in inefficient gas exchange between pregnant mice and fetuses. Under hypoxic or malperfusion conditions, ROS levels was increased in placentas [17,18], which would worsen placental oxidative stress. The situation in PrxIII−/− maternal mice reached the worst level before and during delivery and resulted in fetal hypoxia and death ultimately.

It is well known that pregnancy is accompanied with an increase of blood volume. Since plasma increases to a greater extent than erythrocyte number, the so-called "physiological anemia" occurs. Higher reticulocyte percentage in pregnant mice reflected such a state in the present study. We noticed that the situation in PrxIII−/− maternal mice was relatively serious as compared with PrxIII+/+ or PrxIII+/− littermates. Our finding added weight to recent report that PrxIII was involved in proerythrocyte differentiation [19].

Although there existed serious oxidative stress in placentas derived from PrxIII−/− maternal mice, we did not find Heinz body in erythrocytes, a marker for hemoglobin oxidation. We hypothesize that Prx I provides compensation for PrxIII deficiency on the following evidence: first, Prx I has been proved to play an important antioxidant role in erythrocytes [20]. Second, PrxIII shares more than 70% amino acid sequences with PrxI, and the two Prxs remove H_2O_2 through the same mechanism [4]. Third, the present study indicated that PrxI was significantly up-regulated in erythrocytes of pregnant PrxIII−/− mice. It might be Prx I enhancement that contributed to protection of erythrocytes against oxidative damage.

Acknowledgements: We are very grateful to Miss Kyoko Itoh for help with preparation of this manuscript.

References

[1] Watabe, S., Hiroi, T., Yamamoto, Y., Fujooka, Y., Hasegawa, H., Yago, N. and Takahashi, S.Y. (1997) SP-22 is a thioredoxin-dependent peroxide reductase in mitochondria. Eur. J. Biochem. 249, 52–60.

[2] Chae, H.Z., Kim, H.J., Kang, S.W. and Rhee, S.G. (1999) Characterization of three isoforms of mammalian peroxiredoxin that reduce peroxides in the presence of thioredoxin. Diabetes Res. Clin. Pract. 45, 101–112.

[3] Rabilloud, T., Heller, M., Rigobello, M.P., Bindoli, A., Aebersold, R. and Lunardi, J. (2001) The mitochondrial antioxidant defence system and its response to oxidative stress. Proteomics 1, 1105–1110.

[4] Rhee, S.G., Kang, S.W., Chang, T.S., Jeong, W. and Kim, K. (2001) Peroxiredoxin, a novel family of peroxidases. IUBMB Life 52, 35–41.

[5] Li, L., Shoji, W., Takano, H., Nishimura, N., Aoki, Y., Takahashi, R., Goto, S., Kaifu, T., Takai, T. and Obinata, M. (2007) Increased susceptibility of MER5 (peroxiredoxin III) knockout mice to lipopolysaccharide (LPS)-induced oxidative stress. Biochem. Biophys. Res. Commun. 355, 715–721.

[6] Ejima, K., Nanri, H., Araki, M., Koji, T., Shibata, E., Kashimura, M. and Ikeda, M. (2000) Expression of mitochondrial thioredoxin-dependent antioxidant protein, SP-22, in normal human and inflammatory mouse placentae. Placenta 21, 847–852.

[7] Shibata, E., Nanri, H., Ejima, K., Araki, M., Fukuda, J., Yoshimura, K., Toki, N., Ikeda, M. and Kashimura, M. (2003) Enhancement of mitochondrial oxidative stress and up-regulation of antioxidant protein peroxiredoxin III/SP-22 in the mitochondria of human pre-eclamptic placentae. Placenta 24, 698–705.

[8] Raijmakers, M.T., Roes, E.M., Poston, L., Steegers, E.A. and Peters, W.H. (2007) The transient increase of oxidative stress during normal pregnancy is higher and persists after delivery in women with pre-eclampsia. Eur. J. Obstet. Gynecol. Reprod. Biol., (Epub ahead of print).

[9] Cindrova-Davies, T., Yung, H.W., Johns, J., Spasic-Boskovic, O., Korolchuk, S., Jauniaux, E., Burton, G.J. and Charnock-Jones, D.S. (2007) Oxidative stress, gene expression, and protein changes induced in the human placenta during labor. Am. J. Pathol. 171, 1168–1179.

[10] Qanungo, S. and Mukherjea, M. (2000) Ontogenic profile of some antioxidants and lipid peroxidation in human placental and fetal tissues. Mol. Cell. Biochem. 215, 11–19.

[11] Carone, D., Loverro, G., Greco, P., Capuano, F. and Selvaggi, L. (1993) Lipid peroxidation products and antioxidant enzymes in red blood cells during normal and diabetic pregnancy. Eur. J. Obstet. Gynecol. Reprod. Biol. 51, 103–109.

[12] Roberts, J.M. and Lain, K.Y. (2002) Recent Insights into the pathogenesis of pre-eclampsia. Placenta 23, 359–372.

[13] Toyokuni, S., Miyake, N., Hiai, H., Hagiwara, M., Kawakishi, S., Osawa, T. and Uchida, K. (1995) The monoclonal antibody specific for the 4-hydroxy-2-nonenal histidine adduct. FEBS Lett. 359, 189–191.

[14] Hung, T.H., Charnock-Jones, D.S., Skepper, J.N. and Burton, G.J. (2004) Secretion of tumor necrosis factor-alpha from human placental tissues induced by hypoxia-reoxygenation causes endothelial cell activation in vitro: a potential mediator of the inflammatory response in preeclampsia. Am. J. Pathol. 164, 1049–1061.

[15] Ruef, J., Moser, M., Kubler, W. and Bode, C. (2001) Induction of endothelin-1 expression by oxidative stress in vascular smooth muscle cells. Cardiovasc. Pathol. 10, 311–315.

[16] Kaehler, J., Sill, B., Koester, R., Mittmann, C., Orzechowski, H.D., Muenzel, T. and Meinertz, T. (2002) Endothelin-1 mRNA and protein in vascular wall cells is increased by reactive oxygen species. Clin. Sci. Lond 103, 176S–178S.

[17] Hung, T.H., Skepper, J.N. and Burton, G.J. (2001) In vitro ischemia-reperfusion injury in term human placenta as a model for oxidative stress in pathological pregnancies. Am. J. Pathol. 159, 1031–1043.

[18] Hung, T.H. and Burton, G.J. (2006) Hypoxia and reoxygenation: a possible mechanism for placental oxidative stress in preeclampsia. Taiwan J. Obstet. Gynecol. 45, 189–200.

[19] Yang, H.Y., Jeong, D.K., Kim, S.H., Chung, K.J., Cho, E.J., Yang, U., Lee, S.R. and Lee, T.H. (2007) The role of peroxiredoxin III on late stage of proerythrocyte differentiation. Biochem. Biophys. Res. Commun. 359, 1030–1036.

[20] Neumann, C.A., Krause, D.S., Carman, C.V., Das, S., Dubey, D.P., Abraham, J.L., Bronson, R.T., Fujiwara, Y., Orkin, S.H. and Van Etten, R.A. (2003) Essential role for the peroxiredoxin Prdx1 in erythrocyte antioxidant defence and tumour suppression. Nature 424, 561–565.

Jpn J Clin Oncol 2008;38(12)793–802
doi:10.1093/jjco/hyn116

Review Article

Polymeric Micellar Delivery Systems in Oncology

Yasuhiro Matsumura

Investigative Treatment Division, Research Center for Innovative Oncology, National Cancer Center Hospital East, Kashiwa, Chiba, Japan

Received September 1, 2008; accepted September 22, 2008; published online November 6, 2008

The purpose of drug delivery systems in cancer chemotherapy is to achieve selective delivery of anti-cancer agents to cancer tissue at an effective concentrations for the appropriate duration of time, so that we may be able to reduce the adverse effects of a drug and simultaneously enhance the anti-tumor effect. Polymeric micelles were expected to increase the accumulation of drugs in tumor tissues utilizing the enhanced permeability and retention effect and to incorporate various kinds of drugs into the inner core by chemical conjugation or physical entrapment with relatively high stability. The size of the micelles can be controlled within the diameter range of 20–100 nm, to ensure that the micelles do not pass through normal vessel walls; therefore, a reduced incidence of the side effects of the drugs may be expected due to the decreased volume of distribution. There are several anti-cancer agent-incorporated micelle carrier systems under clinical evaluation. Phase 1 studies of a cisplatin-incorporated micelle, NC-6004 and an SN-38-incorporated micelle, NK012, are now underway. A Phase 2 study of a paclitaxel-incorporated micelle, NK105, against stomach cancer is also underway.

Key words: DDS – polymer micelles – clinical trial – EPR effect

INTRODUCTION

There are two main concepts in drug delivery system (DDS), active targeting and passive targeting. Active targeting involves monoclonal antibodies or ligands to tumor-related receptors, which can target the tumor by utilizing the specific binding ability between the antibody and antigen or between the ligand and its receptor. However, the application of DDS using monoclonal antibodies is restricted to tumors expressing high levels of related antigens. The passive targeting system can be achieved by the enhanced permeability and retention (EPR) effect (1). The EPR effect is based on the pathophysiological characteristics of solid tumor tissues: hypervascularity, incomplete vascular architecture, secretion of vascular permeability factors stimulating extravasation within cancer tissue and absence of effective lymphatic drainage from tumors, which impedes the efficient clearance of macromolecules accumulated in solid tumor tissues.

Several techniques to use maximally the EPR effect have been developed, e.g. modification of drug structures and development of drug carriers. Polymeric micelle-based anti-cancer drugs were originally developed by Prof Kataoka et al. (2–4) in the late 1980s or early 1990s. Polymeric micelles were expected to increase the accumulation of drugs in tumor tissues utilizing the EPR effect and to incorporate various kinds of drugs into the inner core by chemical conjugation or physical entrapment with relatively high stability. The size of the micelles can be controlled within the diameter range of 20–100 nm, to ensure that the micelles do not pass through normal vessel walls; therefore, a reduced incidence of the adverse effects of the drugs may be expected.

In this article, polymeric micelle systems for which clinical trials are now underway are reviewed.

For reprints and all correspondence: Yasuhiro Matsumura, Investigative Treatment Division, Research Center for Innovative Oncology, National Cancer Center Hospital East, Kashiwa, Chiba, Japan. E-mail: yhmatsum@east.ncc.go.jp

NK105, PACLITAXEL-INCORPORATING MICELLAR NANOPARTICLE

Background

Paclitaxel (PTX) is one of the most useful anti-cancer agents known for various cancers, including ovarian, breast and lung cancers (5,6). However, PTX has serious adverse effects, e.g. neutropenia and peripheral sensory neuropathy. In addition, anaphylaxis and other severe hypersensitive reactions have

been reported to develop in 2–4% of patients receiving the drug even after premedication (P) with anti-allergic agents; these adverse reactions have been attributed to the mixture of Cremophor EL and ethanol which was used to solubilize PTX (7,8). Of the adverse reactions, neutropenia can be prevented or managed effectively by administering a granulocyte colony-stimulating factor. On the other hand, there are no effective therapies to prevent or to reduce nerve damage, which is associated with peripheral neuropathy caused by PTX; therefore, neurotoxicity constitutes a significant dose-limiting toxicity (DLT) of the drug (9,10).

Preclinical Study

To construct NK105 micellar nanoparticles (Fig. 1), block copolymers consisting of polyethylene glycol and polyaspartate, the so-called PEG–polyaspartate described previously (2–4,11), were used. PTX was incorporated into polymeric micelles formed by physical entrapment utilizing hydrophobic interactions between PTX and the block copolymer polyaspartate chain (12).

Pharmacokinetic study showed that NK105 exhibited slower clearance from the plasma than PTX. The plasma concentration at 5 min (C_{5min}) and the area under the curve (AUC) of NK105 were 11- to 20-fold and 50- to 86-fold higher for NK105 than that for PTX, respectively. The maximum concentration (C_{max}) and AUC of NK105 in Colon 26 tumors were ~three times and 25 times higher for NK105 than that for PTX, respectively. NK105 continued to accumulate in the tumors until 72 h after injection (12). In *in vivo* anti-tumor activity, BALB/c mice bearing s.c. HT-29 colon cancer tumors showed decreased tumor growth rates after the administration of PTX and NK105. However, NK105 exhibited superior anti-tumor activity as compared with PTX ($P < 0.001$). The anti-tumor activity of NK105 administered at a PTX-equivalent dose of 25 mg/kg was comparable to that obtained after the administration of free PTX 100 mg/kg. Tumor suppression by NK105 increased in a dose-dependent manner. Tumors disappeared after the first dosing to mice treated with NK105 at a PTX-equivalent dose of 100 mg/kg, and all mice remained tumor-free thereafter (Fig. 2). In addition, less weight loss was induced in mice

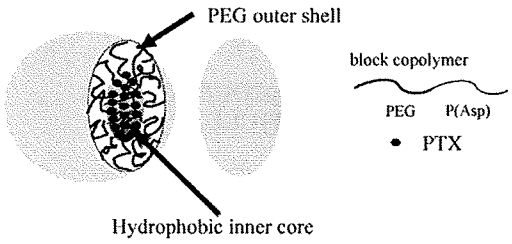

Figure 1. Preparation and characterization of NK105. The micellar structure of NK105 paclitaxel (PTX) was incorporated into the inner core of the micelle. PEG, polyethylene glycol (12).

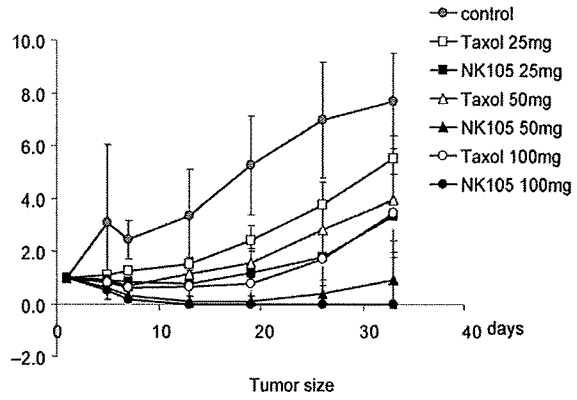

Figure 2. Effects of PTX (open symbols) and NK105 (closed symbols). PTX and NK105 were injected intravenously once weekly for 3 weeks at PTX-equivalent doses of 25 mg/kg (open square, closed square), 50 mg/kg (open triangle, closed triangle) and 100 mg/kg (open circle, closed circle), respectively. Saline was injected to control animals (open square) (12).

given NK105 100 mg/kg than in those given the same dose of free PTX (12).

Treatment with PTX has resulted in cumulative sensory-dominant peripheral neurotoxicity in humans, characterized clinically by numbness and/or paraesthesia of the extremities. Pathologically, axonal swelling, vesicular degeneration and demyelination were observed. We, therefore, examined the effects of free PTX and NK105 using both electrophysiological and morphological methods. Prior to drug administration, there were no significant differences in the amplitude of caudal sensory nerve action potential between two drug administration groups. The amplitude was significantly smaller in the PTX group than in the control group ($P < 0.01$), while the amplitude was significantly larger in the NK105 group than in the PTX group ($P < 0.05$) and was comparable between the NK105 group and the control group (Fig. 3).

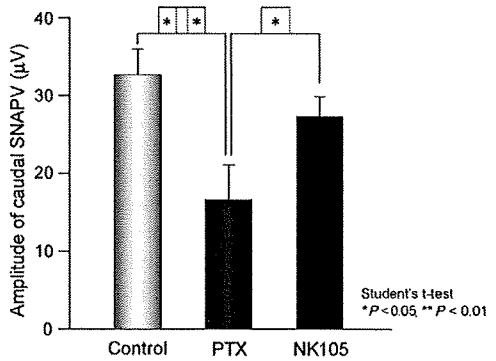

Figure 3. Effects of PTX or NK105 on the amplitude of rat caudal sensory nerve action potentials as examined 5 days after weekly injections for 6 weeks. Rats ($n = 14$) were injected with NK105 or PTX at a PTX-equivalent dose of 7.5 mg/kg. Five percent glucose was also injected in the same manner to animals in the control group (12).

CLINICAL STUDY

A Phase 1 study was designed to determine maximum tolerated dose (MTD), DLTs, the recommended dose (RD) for Phase 2 and the pharmacokinetics of NK105 (13). NK105 was administered by 1-h intravenous infusion every 3 weeks without anti-allergic P. The starting dose was 10 mg PTX-equivalent/m^2, and dose escalated according to the accelerated titration method. Nineteen patients were treated at the following doses: 10 ($n = 1$), 20 ($n = 1$), 40 ($n = 1$), 80 ($n = 1$), 110 ($n = 3$), 150 ($n = 7$) and 180 mg/m^2 ($n = 5$). Tumor types treated have included: pancreatic ($n = 11$), bile duct ($n = 5$), gastric ($n = 2$) and colon ($n = 1$). Neutropenia has been the predominant hematological toxicity and Grade 3 or 4 neutropenia was observed in patients treated at 110, 150 and 180 mg/m^2. One patient at 180 mg/m^2 developed Grade 3 fever. No other Grade 3 or 4 non-hematological toxicity including neuropathies was observed. DLTs were observed in two patients at the 180 mg/m^2 (Grade 4 neutropenia lasting for more than 5 days), which was determined as MTD. Allergic reactions were not observed in any of the patients except in one patient at 180 mg/m^2. A partial response was observed in one pancreatic cancer patient, who received more than 12 courses of NK105 (13) (Fig. 4). Despite the long-time usage, only Grade 1 or 2 neuropathy was observed by modifying the dose or period of drug administration. Colon and gastric cancer patients experienced stable disease lasting 10 and 7 courses, respectively. The C_{max} and AUC of NK105 showed dose-dependent characteristics. The plasma AUC of NK105 at 180 mg/m^2 was ~30-fold higher than that of the commonly used PTX formulation (13) (Fig. 5). DLT was Grade 4 neutropenia. NK105 generates prolonged systemic exposure to PTX in plasma. Tri-weekly 1-h infusion of NK105 was feasible and well tolerated, with anti-tumor activity in pancreatic cancer patients. A Phase 2 study of NK105 is now underway against advanced stomach cancer as a second line therapy.

NC-6004, CISPLATIN-INCORPORATING MICELLAR NANOPARTICLE

BACKGROUND

Cisplatin [*cis*-dichlorodiammineplatinum (II): CDDP] is a key drug in the chemotherapy for cancers, including lung, gastrointestinal and genitourinary cancer (14,15). However, we often find that it is necessary to discontinue treatment with CDDP due to its adverse reactions, e.g. nephrotoxicity and neurotoxicity, despite its persisting effects (16). Platinum analogues, e.g. carboplatin and oxaliplatin (17), have been developed to date to overcome these CDDP-related disadvantages. Consequently, these analogues are becoming the standard drugs for ovarian (18) and colon cancers (19). However, those regimens including CDDP are considered to constitute the standard treatment for lung, stomach, testicular (20) and urothelial cancers (21). Therefore, the development of a DDS technology is anticipated, which would offer the better selective accumulation

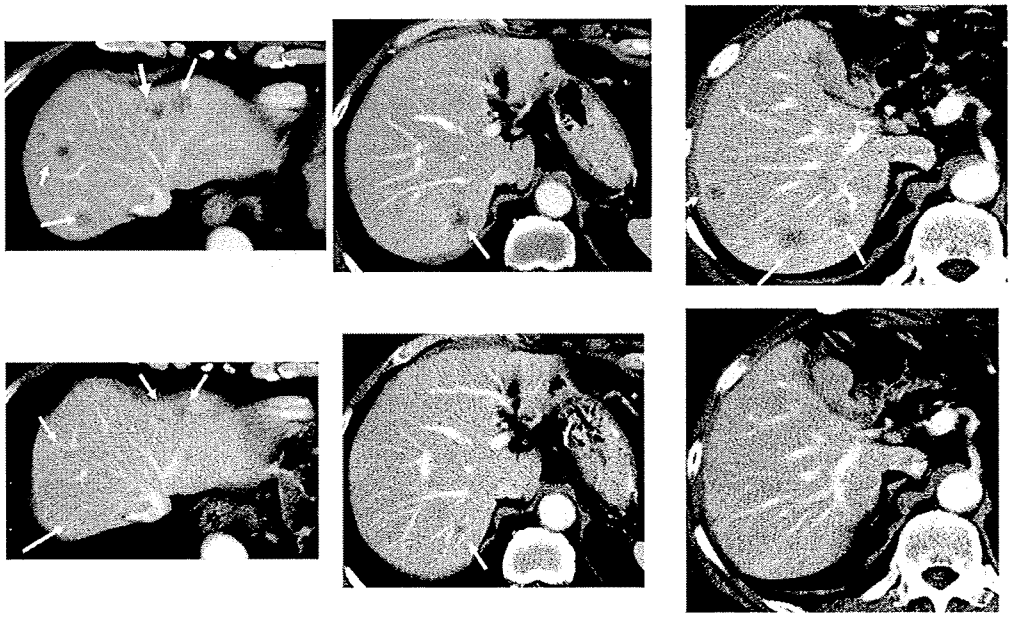

Figure 4. Serial computed tomography (CT) scans. A 60-year-old male with pancreatic cancer, who was treated with NK105 at a dose level of 150 mg/m^2. Baseline scan (upper panels) showing multiple metastasis in the liver. Partial response, characterized by a more than 90% decrease in the size of the liver metastasis (lower panels) compared with the baseline scan. The anti-tumor response was maintained for nearly 1 year (13).

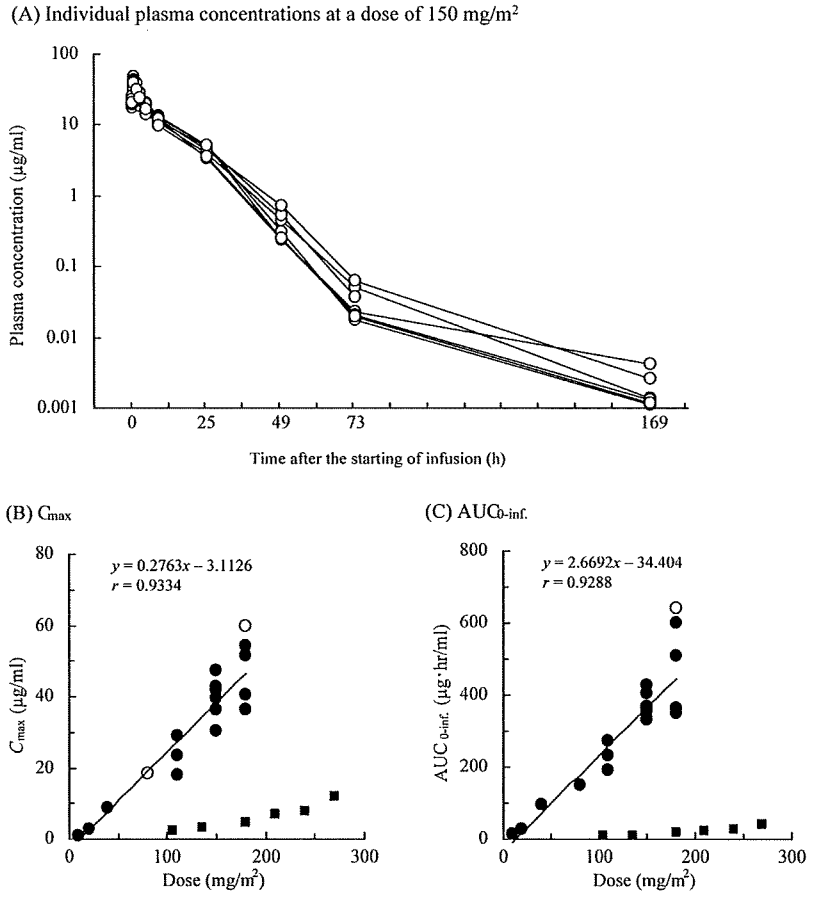

Figure 5. (A) Individual plasma concentrations of PTX in seven patients following 1 h intravenous infusion of NK105 at a dose of 150 mg/m^2. Relationships between dose and C_{max} (B), and between dose and AUC0-inf. (C) of PTX in patients following 1 h intravenous infusion of NK105. Regression analysis for dose versus C_{max} was applied using all points except for one patient at 80 mg/m^2 whose medication time became 11 min longer and one patient at 180 mg/m^2 who had medication discontinuation and steroid medication (open circle). Regression analysis for dose vs. AUC0-inf. was applied using all points except for one patient who had medication discontinuation and steroid medication (closed circle). Relationships between dose and C_{max}, and AUC0-inf in patients following conventional PTX administration were plotted (closed square) (13).

of CDDP into solid tumors while lessening its distribution into normal tissue.

Preclinical Study

NC-6004 consists of PEG, a hydrophilic chain that constitutes the outer shell of the micelles, and the coordinate complex of poly(glutamic acid) [P(Glu)] and CDDP, a polymer–metal complex-forming chain that constitutes the inner core of the micelles (22) (Fig. 6). The molecular weight of PEG-P(Glu) as a sodium salt was ~18 000 [PEG: 12 000; P(Glu): 6000]. The release rates of CDDP from NC-6004 were 19.6 and 47.8% at 24 and 96 h, respectively. In distilled water, furthermore, NC-6004 was stable without releasing cisplatin.

The AUC_{0-t} and C_{max} values were significantly higher in animals given NC-6004 than in animals given CDDP, namely, 65- and 8-fold, respectively ($P < 0.001$ and 0.001, respectively) (23). The C_{max} in tumor was 2.5-fold higher for NC-6004 than for CDDP ($P < 0.001$). Furthermore, the tumor AUC was 3.6-fold higher for NC-6004 than for CDDP (81.2 and 22.6 μg/ml h in animals given NC-6004 and CDDP, respectively) (23).

BALB/c nude mice implanted with a human gastric cancer cell line MKN-45 showed decreased tumor growth rates after i.v. injection of CDDP and NC-6004 (Fig. 7A). The NC-6004 administration groups at the same dose levels as CDDP showed no significant difference in tumor growth rate. Regarding time-course changes in body weight change rate, the CDDP 5 mg/kg administration group showed a significant decrease ($P < 0.001$) in body weight as compared with the control group. On the other hand, NC-6004 administration group did not show a decrease in body weight as compared with the control group (Fig. 7B).

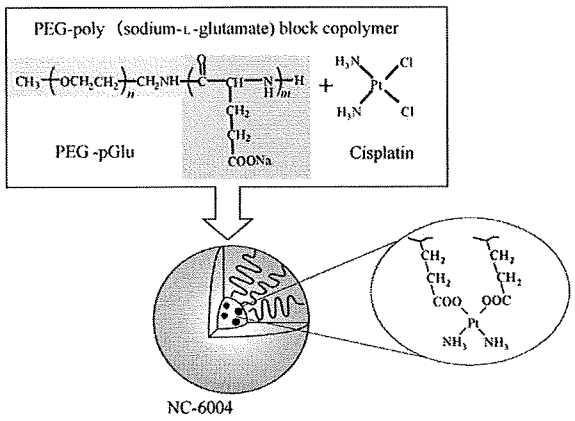

Figure 6. Preparation and characterization of cisplatin (CDDP)-incorporating polymeric micelles (NC-6004). Chemical structures of CDDP and polyethylene glycol poly(glutamic acid) block copolymers [PEG-P(Glu) block copolymers], and the micellar structures of CDDP-incorporating polymeric micelles (NC-6004) (22).

Regarding toxicity, the CDDP 10 mg/kg administration group showed significantly higher plasma concentrations of blood urea nitrogen and creatinine as compared with the control group ($P < 0.05$ and 0.001, respectively), with the NC-6004 10 mg/kg administration group ($P < 0.05$ and 0.001, respectively) (Fig. 8A and B). Light microscopy indicated tubular dilation with flattening of the lining cells of the tubular epithelium in the kidney from all animals in the CDDP 10 mg/kg administration group. On the other hand, no histopathologic change was observed in the kidneys from all animals in the NC-6004 10 mg/kg administration group (data not shown). Animals given NC-6004 showed no delay in sensory nerve condition velocities (SNCVs) as compared with animals given 5% glucose. On the other hand, animals given CDDP showed a significant delay ($P < 0.05$) in SNCV as compared with animals given NC-6004 (Fig. 9A). The analysis by ICP-MS on sciatic nerve concentrations of platinum showed that the concentrations were significantly ($P < 0.05$) lower in animals given NC-6004 (Fig. 9B). This finding is believed to be a factor that reduced neurotoxicity following NC-6004 administration as compared with the CDDP administration (23).

Clinical Study

A Phase 1 trial was run in two UK experimental cancer medicine centers with the PK assays performed in a good laboratory practice-accredited laboratory in Newcastle University (24).

Patients with solid tumors were included in this open-label trial. Usual Phase 1 inclusion and exclusion criteria were applied, including adequate renal function. Patients were limited to one previous course of platinum-based treatment with maximum dose limits of cisplatin, carboplatin or oxaliplatin.

Dose escalation proceeded in two stages. In Stage 1, we recruited cohorts of one to three patients until Grade 2 toxicity was seen in Cycle 1. In Stage 2, we had cohorts of three patients expanding to six if one of three DLT and to confirm MTD.

The starting dose for the Phase 1 study was 10 mg/m^2. NC-6004 was administered as a 60 min infusion with a total infusion volume of 500 ml. Treatment was repeated on a 3-weekly cycle until progressive disease, intolerance of the agent or patient withdrawal. Pharmacokinetic analysis of total plasma platinum (Pt), micellar Pt and ultrafiltrate Pt (UF Pt) was performed using WinNonlin version 1.3 to calculate C_{max}, T_{max}, half-life and AUC for all Pt species. Clearance and volume of distribution were calculated based on the measurements of total and micellar Pt.

In this trial, 17 patients (10 male, 7 female) were treated. The median age (range) was 59 years (40–80), and tumor

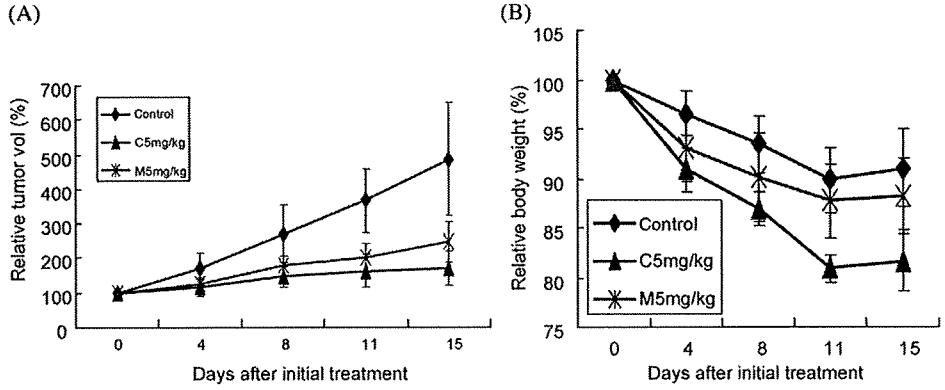

Figure 7. Relative changes in MKN-45 tumor growth rates in nude mice. (A) CDDP (closed triangle) and NC-6004 (cross symbol) were injected intravenously every 3 days, three administrations in total, at CDDP-equivalent doses of 5 mg/kg. Five percent glucose was injected in the control mice (open diamond). (B) Changes in relative body weight. Data were derived from the same mice as those used in the present study. Values are expressed as the mean ± SE (23).